JOURNAL OF PETROLOGY | VOLUME 46 | NUMBER 11 | PAGES 2253–2280 | 2005 | doi:10.1093/petrology/egi054

Geochemistry, Petrogenesis and Metallogenesis of the Panzhihua Gabbroic Layered Intrusion and Associated Fe–Ti–V Oxide Deposits, Sichuan Province, SW China

MEI-FU ZHOU[1]*, PAUL T. ROBINSON[1], C. MICHAEL LESHER[2], REID R. KEAYS[2,3], CHENG-JIANG ZHANG[4] AND JOHN MALPAS[1]

[1]DEPARTMENT OF EARTH SCIENCES, UNIVERSITY OF HONG KONG, POKFULAM ROAD, HONG KONG, PEOPLE'S REPUBLIC OF CHINA

[2]MINERAL EXPLORATION RESEARCH CENTRE, DEPARTMENT OF EARTH SCIENCES, LAURENTIAN UNIVERSITY, SUDBURY, ONTARIO, CANADA P3E 2C6

[3]VIEPS, SCHOOL OF GEOSCIENCES, MONASH UNIVERSITY, VIC. 3800, AUSTRALIA

[4]THIRD DEPARTMENT, CHENGDU UNIVERSITY OF TECHNOLOGY, CHENGDU, PEOPLE'S REPUBLIC OF CHINA

RECEIVED FEBRUARY 11, 2004; ACCEPTED APRIL 19, 2005
ADVANCE ACCESS PUBLICATION MAY 27, 2005

The Panzhihua gabbroic layered intrusion is associated with the 260 Ma Emeishan Large Igneous Province in SW China. This sill-like body hosts a giant Fe–Ti–V oxide deposit with 1333 million ton ore reserves, which makes China a major producer of these metals. The intrusion has a Marginal zone of fine-grained hornblende-bearing gabbro and olivine gabbro, followed upward by Lower, Middle, and Upper zones. The Lower and Middle zones consist of layered melanogabbro and gabbro composed of cumulate clinopyroxene, plagioclase, and olivine. These zones also contain magnetite layers. The Upper zone consists chiefly of leucogabbro composed of plagioclase and clinopyroxene with minor olivine. Most rocks in the body show variable-scale rhythmic modal layering in which dark minerals, primarily clinopyroxene, dominate in the lower parts of each layer, and lighter minerals, primarily plagioclase, dominate in the upper parts. The oxide ores occur as layers and lenses within the gabbros and are concentrated in the lower parts of the intrusion. Ore textures and associated mineral assemblages indicate that the ore bodies formed by very late-stage crystallization of V-rich titanomagnetite from an immiscible oxide liquid in a fluid-rich environment. The rocks of the Panzhihua intrusion become more evolved in chemistry upward and follow a tholeiitic differentiation trend with enrichment in Fe, Ti, and V. They are enriched in light rare earth elements relative to heavy rare earth elements, and exhibit positive Nb, Ta, and Ti anomalies and negative Zr and Hf anomalies. The silicate rocks and oxide ores of the Panzhihua intrusion formed from highly evolved Fe–Ti–V-rich ferrobasaltic or ferropicritic magmas. The textures of the ores and the abundance of minor hydrous phases indicate that addition of fluids from upper crustal wall-rocks induced the separation of the immiscible oxide melts from which the Fe–Ti–V oxide ore bodies in the lower part of the intrusion crystallized.

KEY WORDS: *magnetite; Fe–Ti-rich gabbro; layered intrusion; Panzhihua; SW China*

INTRODUCTION

Layered intrusions are key to understanding the genesis and chemical evolution of mafic–ultramafic magmas and the processes associated with the formation of Cr, Fe–Ti–(V), and platinum group element (PGE) deposits (e.g. Wager & Brown, 1968; Irvine, 1975; Parsons, 1987; Cawthorn, 1996; Keays *et al.*, 1999; Cabri, 2002, and references therein). Nevertheless, the mechanisms by which millions of tonnes of Fe, Cr, Ti and V become concentrated to form massive chromitites and Fe–Ti oxide deposits remain poorly understood. For example,

*Corresponding author. Telephone: 852 2857 8251. E-mail: mfzhou@hkucc.hku.hk

although stratiform chromitites, such as those of the Bushveld and Stillwater complexes, are considered by many researchers to have formed by magma mixing and/or crustal contamination in dynamic layered intrusions (Campbell, 1977; Irvine, 1977; Kinnaird *et al.*, 2002), the precise mechanisms by which the oxides crystallized and accumulated remain unclear.

There are two types of temporally and spatially associated intrusions within the 260 Ma Emeishan Large Igneous Province (ELIP); namely, small ultramafic subvolcanic sills that host magmatic Fe–Ni–Cu–(PGE)-bearing sulfide deposits and large mafic layered intrusions that host giant Fe–Ti–V oxide deposits. It has been shown that the sulfide-bearing intrusions represent magma conduits for the Emeishan flood basalts (Zhou *et al.*, 2002*a*; Song *et al.*, 2003), but the significance of the larger intrusions is unclear. The Panzhihua Fe–Ti–V oxide mine has been a major source of V, Ti, and Fe since the 1960s and makes China a major producer of these metals, accounting for 6·7% and 35·2% of the total world production of V and Ti, respectively. It has thus far produced over 134 million tons (Mt) of ore containing an average of 45 wt % FeO, 12 wt % TiO_2, and 0·3 wt % V_2O_5, and currently contains 1199 million tons of ore (Ma *et al.*, 2003). Similar occurrences of such deposits include those in the Ushushwana and Rooiwater complexes in South Africa (Winter, 1965; Reynolds, 1978). Genetic and exploration models for such deposits are poorly constrained, despite their tremendous economic significance. Likewise, the relationship between the Fe–Ti–V oxide orebodies and their host rocks is not known.

Open pit and underground mining operations are still active in Panzhihua, providing an excellent opportunity for detailed sampling. The Panzhihua intrusion is thus ideal for examining the mechanisms by which the melts evolved and the metals concentrated. The intrusion was previously considered to be of Early Paleozoic age based on Rb–Sr and K–Ar ages ranging from 400 to 560 Ma (Zhang *et al.*, 1988; SBGMR, 1991). However, dating of zircons from this intrusion using the sensitive high-resolution ion microprobe (SHRIMP) technique places the age at ~260 Ma, which is identical to that of other intrusions within the ELIP (Zhou *et al.*, 2002*c*). In this paper, we present the results of the first detailed field and laboratory study of the Panzhihua intrusion and its ore deposits. We use a range of new geochemical data to constrain the composition of the parental magma, to investigate the processes of fractionation and mineralization, and to link the Panzhihua body to other intrusions within the ELIP.

GEOLOGICAL BACKGROUND

Regional geology

Southwest China comprises the Yangtze Block in the east and the Tibetan Plateau in the west (Fig. 1). The easternmost part of the Tibetan Plateau is represented by the Songpan–Ganze terrane, which contains SE-verging, Late Triassic–Early Jurassic thrust belts and is characterized by a thick (up to 10 km or more) sequence of Late Triassic deep marine strata (Burchfiel *et al.*, 1995).

The Yangtze Block contains a lower sequence of Late Mesoproterozoic to Silurian strata, a middle sequence of Devonian to Triassic strata, and an upper sequence of Jurassic and younger strata. The lower and middle sequences are basically marine sedimentary rocks, whereas the upper sequence contains mostly terrestrial basin deposits. The western margin of the Yangtze Block is marked by abundant Neoproterozoic granites and associated metamorphic complexes, known as the Kangdian complexes, which were probably uplifted at ~175 Ma (Zhou *et al.*, 2002*b*; Yan *et al.*, 2003). During the Cenozoic, block-faulting and shallow-level shearing dominated in the eastern part of the Yangtze Block, whereas thrusting and strike-slip faulting dominated in the western part (Burchfiel *et al.*, 1995).

Emeishan Large Igneous Province

The ELIP covers an area of 5×10^5 km^2 in SW China and northern Vietnam, and includes the Emeishan Continental Flood Basalts and associated mafic–ultramafic intrusions in the western part of the Yangtze Block and the eastern margin of the Tibetan Plateau. The Emeishan volcanic succession ranges from several hundred meters to 5 km in thickness (Chung & Jahn, 1995; Song *et al.*, 2001; Xu *et al.*, 2001) and consists primarily of picrites, tholeiitic basalts, and basaltic andesites. The parental melts are believed to have been derived from a mantle plume and to have been contaminated by interaction at relatively shallow depths with enriched lithospheric mantle (Song *et al.*, 2001). Enrichment of the lithosphere suggests that the mantle was modified by ancient subduction of an oceanic slab (Song *et al.*, 2001).

In the western part of the ELIP, the volcanic succession has been strongly deformed, uplifted, and eroded as a result of the India–Eurasia collision during the Cenozoic. In the Panxi (Panzhihua–Xichang) district along the western margin of the Yangtze Block (Fig. 1), several north–south-trending faults have exposed Emeishan dykes and large intrusions over a considerable range of emplacement depths. Several of these bodies, such as the Xinjie, Baima, Panzhihua and Limahe intrusions, and the Miyi syenite complex have been dated at ~259 to 263 Ma (Zhou *et al.*, 2002*c*, in preparation). This western region is the most important Fe–Ti–V metallogenic district in China (Zhong *et al.*, 2002, 2003; Ma *et al.*, 2003). The ore-bearing mafic and ultramafic rock bodies extend from Mianning in the north, through Xichang, Miyi, and Panzhihua in Sichuan Province, to Mouding in Yunnan Province in the south (Fig. 1). They constitute a mineralized zone about 300 km long and 10–30 km

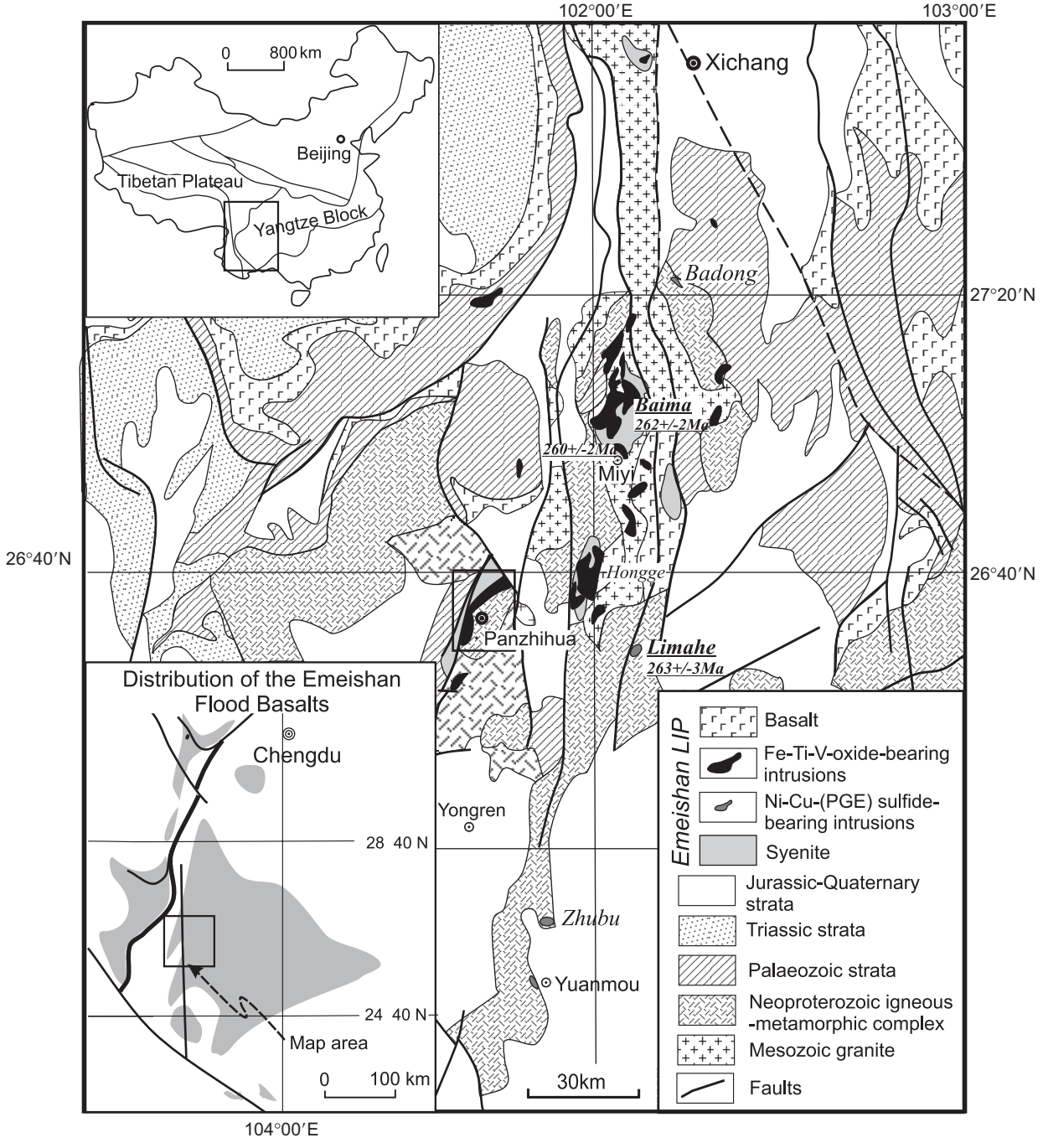

Fig. 1. Regional geological map showing the distribution of the Emeishan flood basalts in SW China and northern Vietnam, and related mafic intrusions in the Panxi district, Sichuan Province, SW China [modified after Zhang *et al.* (1988)]. Ages of some of the intrusions are the authors' unpublished SHRIMP zircon dating results.

wide, previously referred to as the Panxi rift zone (Zhang *et al.*, 1988). Three large Fe–Ti–V oxide ore deposits have been explored in the Panxi District: Panzhihua (1333 Mt ore reserves), Baima (1497 Mt ore reserves), and Hongge (4572 Mt ore reserves) (Ma *et al.*, 2003), but only the Panzhihua Fe–Ti–V oxide mine is currently active.

PANZHIHUA GABBROIC INTRUSION

Field relationships

The Panzhihua gabbroic intrusion is a sill-like body that dips 50–60° NW and extends NE–SW along strike for about 19 km. It is ~2 km thick and has an outcrop area

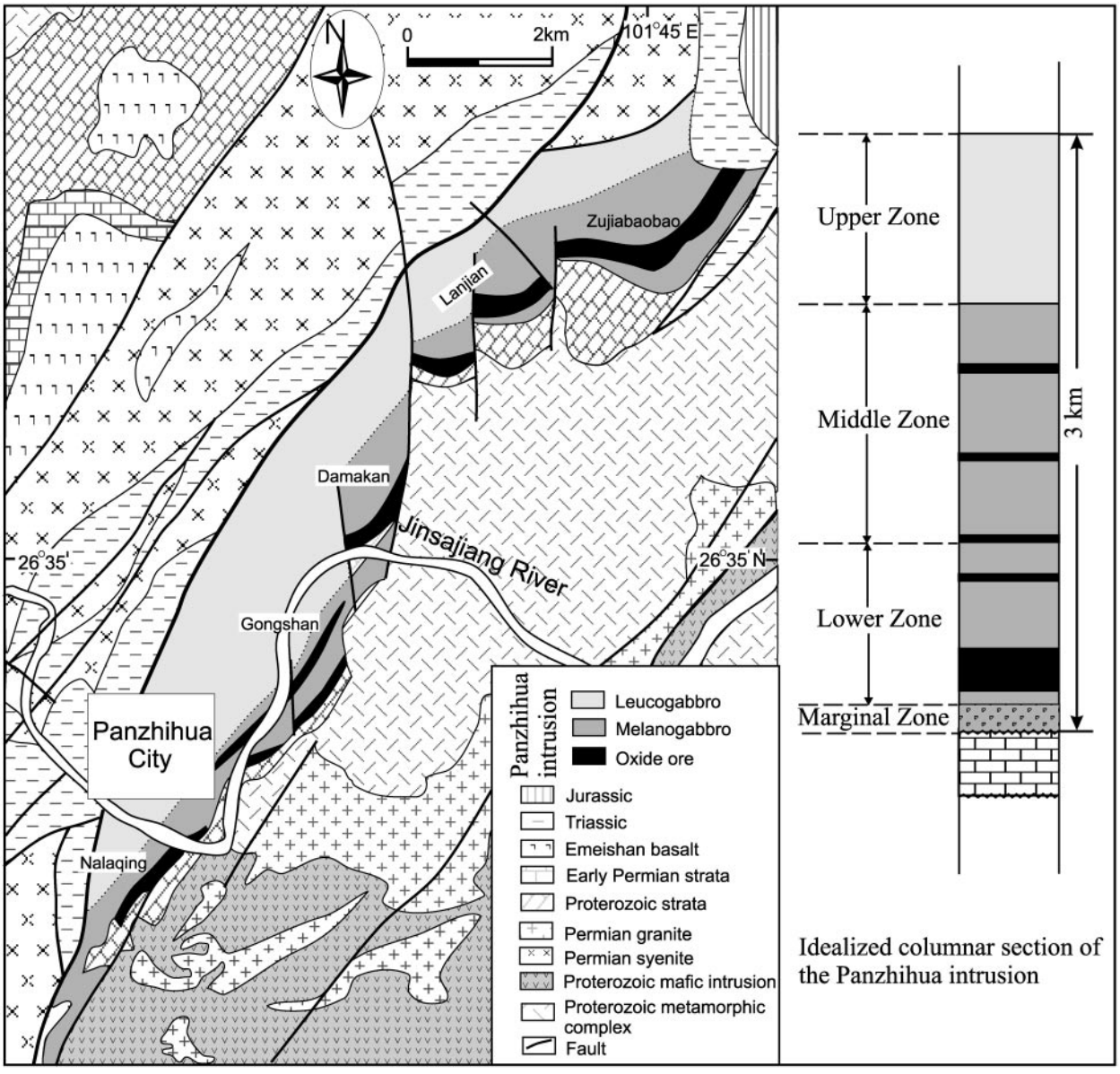

Fig. 2. Geological map of the Panzhihua intrusion, SW China (after Tang, 1984). The insert is an idealized columnar section. Samples used in this study were collected along a cross-section in Lanjian.

of ~30 km^2 (Fig. 2). The ore-bearing gabbroic body concordantly intruded dolomitic limestones of the Late Neoproterozoic Dengying Formation, which were metamorphosed to forsterite and diopside marbles along the contact and form the footwall of the intrusion. The hanging-wall rocks include Late Permian syenites and Triassic shales and coal measures, which are in fault contact with the intrusion. This contact dips NW and is interpreted as a thrust fault.

The Panzhihua intrusion is transected by steeply dipping, north-trending faults that cut the ore horizons into several blocks that are currently being mined; for example, the Zujiabaobao, Lanjian, Damakan, Gongshan, and Nalaqing mines (Fig. 2).

Lithology and stratigraphic subdivision

Despite extensive regional tectonic activity associated with the Cenozoic Indian–Eurasian collision, the Panzhihua intrusion is generally undeformed and unmetamorphosed, except along local shear zones and marginal zones. Based on differences in internal structure and the extent of oxide mineralization, local geologists previously identified four zones in the intrusion: a

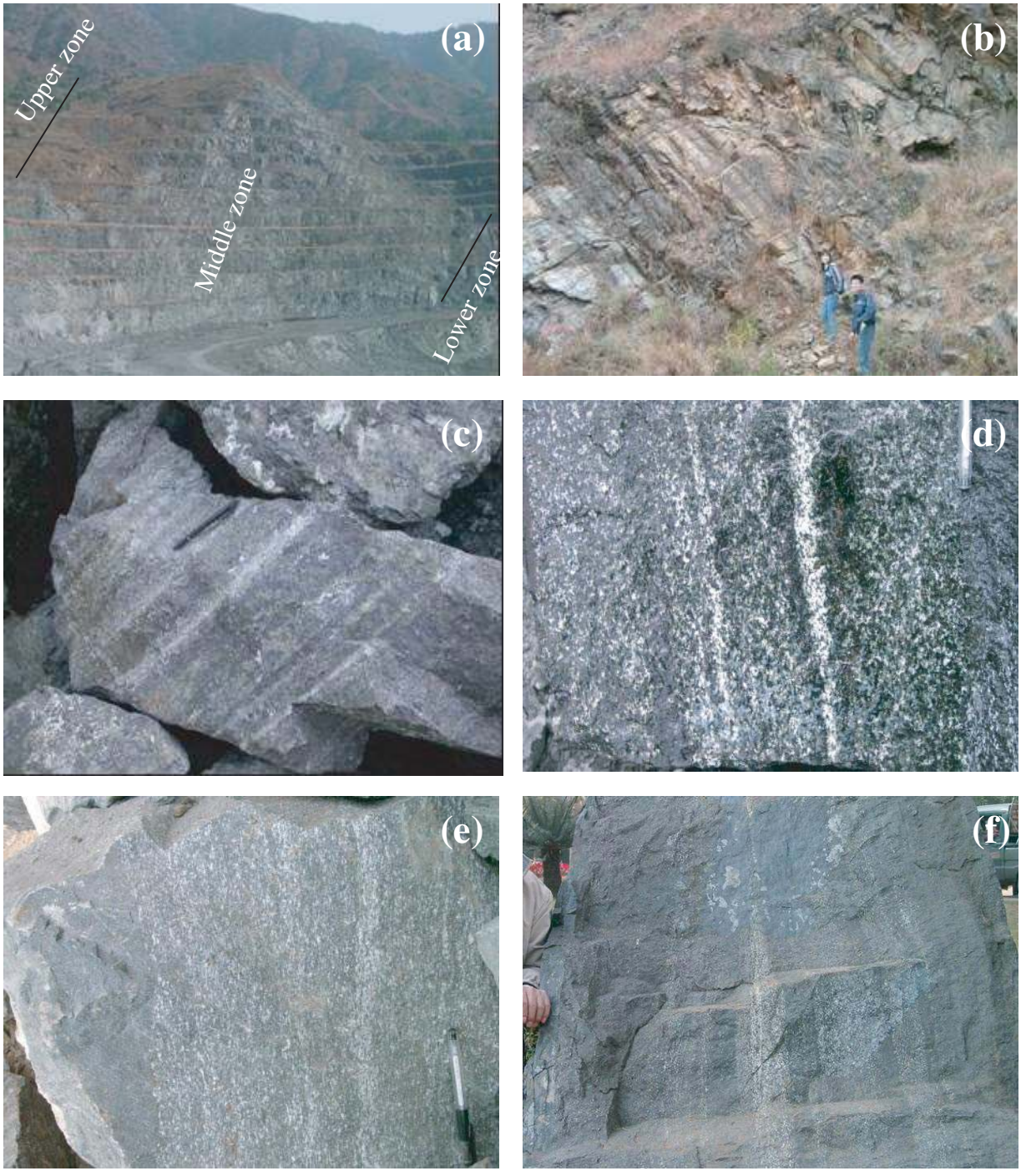

Fig. 3. Field photographs of layered structures in the Panzhihua intrusion, SW China. (a) Three zones are clearly visible in the Zujiabaobao mine, viewed to the NE; (b) layered structure in the lower part of the Upper zone, viewed to the south; (c) rhythmic layering of a melanogabbro; (d) rhythmic layering of melanogabbro to leucogabbro; (e) layering of melanogabbro, showing a sharp boundary and mineral foliation; (f) layered structure of an oxide ore. White mineral is plagioclase.

Marginal zone at the base, followed upward by Lower, Middle, and Upper zones (Figs 2 and 3a, b). The Marginal zone is 0–40 m thick, very heterogeneous, and consists of fine-grained hornblende-bearing gabbro and olivine gabbro with abundant marble xenoliths derived from the footwall. The Lower zone ranges from 0 to 110 m in thickness and is composed of layered melanogabbros (Fig. 3c and d) with major oxide layers

(the ore bodies) up to 60 m thick. The Middle zone is up to 800 m thick and consists of layered gabbro (Fig. 3e) with some oxide ore bodies, whereas the Upper zone, with a thickness of 500–1500 m, consists mainly of unmineralized leucogabbro (Fig. 3b). Small amounts of anorthosite, syenite, granophyre, and felsic pegmatite also occur as dykes or lenses within the intrusion.

The division of the intrusion into four zones was adopted by the mining geologists for mineral exploration purposes and does not accurately reflect variations in cumulus or intercumulus mineralogy. It does, however, reflect some general differences in the nature of layering and the abundance of ore bodies. For example, the uppermost part of the Upper zone is not as well layered as the lower units and lacks oxide deposits. The Middle zone is characterized by abundant oxide layers and is rich in apatite, whereas the Lower zone contains the largest and most abundant oxide layers.

Most of the gabbros are medium- to coarse-grained with local pegmatitic facies. The melanogabbros are dark, coarse-grained rocks composed of approximately 50 modal % clinopyroxene, 40 modal % plagioclase, up to 12 modal % olivine and a few percent each of magnetite and hornblende (Table 1). Some rocks in the Middle zone also contain up to 5 modal % apatite. Plagioclase and clinopyroxene are typically euhedral and up to about 10 mm in length, whereas interstitial magnetite generally forms anhedral grains up to 4 mm long (Fig. 4a and b). Leucogabbros are somewhat finer-grained and characterized by abundant white plagioclase crystals up to 5 mm long. A typical mode consists of plagioclase 60–70%, clinopyroxene 25–30%, hornblende 2–3%, magnetite up to 5% (Table 1). Some samples also contain small amounts of olivine. The anorthosites are medium- to coarse-grained rocks with ~90 modal % plagioclase, ~5 modal % clinopyroxene, and ~5 modal % apatite and zircon.

Minor granophyres and felsic pegmatites occur as dykes or lenses within the Panzhihua intrusion. Most common are pegmatitic gabbro dykes, rich in sulfide minerals that occur chiefly in the lower parts of the mineralized gabbros. Less abundant syenite dykes, composed of orthoclase and microcline, also cut the lower parts of the ore-bearing gabbros. Some of these dykes are also pegmatitic with grain sizes up to a few centimeters. Anorthositic dykes cut the Middle and the Upper zones. A few dioritic dykes cut through the entire intrusion, but their relationship, if any, to the main body is unknown.

Internal structure

All but the uppermost part of the intrusion is well layered with features similar to those described in the Skaergaard intrusion (Wager & Brown, 1968; McBirney, 1996) and the Bushveld intrusion (see reviews by Eales & Cawthorn, 1996; Lee, 1996; Cawthorn & Spies, 2003). Both modal layering and grain-size layering are present, but the layering varies in form, frequency, and spacing. Layering is most pronounced in the Lower and Middle zones, where individual bands can be traced laterally for several kilometers.

Rocks within the intrusion are generally rhythmically layered on a centimeter-scale throughout the Lower and Middle zones and lower part of the Upper zone (Fig. 3b–e). Individual layers are about 2–20 cm thick and are oriented parallel to the sill boundaries. Layering is mostly manifested in the modal proportions of dark and light minerals, but in places it also results from variations in grain size and crystal orientation. Although graded layers are common, many layers have alternating bands of dark and light layers. Graded layers typically have a well-defined base and consist of a lower part rich in clinopyroxene and olivine that passes gradually upward into more plagioclase-rich gabbro or even anorthosite.

The mineral grains are typically larger in the lower parts of the intrusion. For example, gabbros in the Upper zone have clinopyroxene ranging in size from 0·1 to 1 mm and plagioclase ranging from 0·1 to 0·6 mm. In the lower units clinopyroxene is between 2 and 10 mm and plagioclase between 1 and 5 mm in diameter. Within individual layers, mineral grains are coarsest in the lower part and decrease in size upward.

In addition to rhythmic layering, many rocks in the Lower and Middle zones show mineral foliation produced by alignment of tabular plagioclase, parallel to the plane of layering (Fig. 3e). This texture is similar to the igneous lamination described in the Skaergaard intrusion and is probably due to deposition of crystals of tabular habit from a moving magma (Wager & Brown, 1968). Igneous lamination in the Panzhihua intrusion is also associated with the ore layers.

Oxide mineralization

The ore bodies in the Panzhihua intrusion are both tabular and lens-shaped. Tabular or layered bodies are the most common and make up the major ore zone at the base of the Lower zone (Fig. 3f). The lenticular bodies have limited lateral extent and occur mostly in the Middle zone. Both types of ore display massive and disseminated textures. The major ore zone in the basal part of the Lower zone extends continuously for more than 15 km along strike and at least 850 m down dip as revealed by drilling. The average ore grade is 43 wt % FeO, 11·68 wt % TiO_2, and 0·30 wt % V_2O_5.

Lens-shaped ore bodies are variable in size and distribution. At Nalaqing, there are 14 such ore bodies with the largest being 160 m long and 30 m wide. At Gongshan, a few small lenticular ore bodies are reported

Table 1: Stratigraphic position and estimated modal mineralogy of the analysed samples from the Panzhihua intrusion, SW China

Lithological zone:	Marginal Zone			Lower Zone									
Sample no.:	Lj-03	Lj-04	Lj-05	Lj-06	Lj-07	Lj-08	Lj-09	Lj-10	Lj-11	Lj-12	Lj-13	Lj-14	Lj-15
Rock name:	Ol Gab	Gab	Gab	Ol Gab	Gab	Gab	Gab	Ore	Ore	Gab	Ore	Gab	Anorth
Meters above base:	15	30	38	45	50	60	70	75	80	86	92	115	135
Plagioclase	53	45	60	20	40	45	35	0	0	65	0	60	90
Clinopyroxene	15	30	17	30	25	15	40	10	23	18	5	32	0
Magnetite	12	12	8	35	17	10	22	85	70	12	80	5	tr
Olivine	12	0	0	12	0	0	0	2	5	0	5	0	2
Amphibole	7	8	15	3	17	30	3	3	2	5	10	3	8
Apatite	1	5	<1	trace	1	<1	trace	0	0	trace	0	trace	trace
Biotite	0	0	tr	0	0	0	0	0	0	0	0	tr	0
Quartz	0	0	0	0	0	0	0	0	0	0	0	0	0
Titanite	0	0	0	0	0	0	0	0	0	0	0	0	0
Epidote	0	0	0	0	0	0	0	0	0	0	0	0	0

Lithological zone:	Middle Zone											
Sample no.:	Lj-16	Lj-17	Lj-18	Lj-19	Lj-20	Lj-21	Lj-22	Lj-23	Lj-24	Lj-25	Lj-26	Lj-27
Rock name:	Gab	Anorth	Ore	Ol Gab	Gab	Ol Gab	Gab	Gab	Gab	Ol Gab	Anorth	Ol Gab
Meters above base:	160	180	190	200	240	275	300	340	375	390	440	470
Plagioclase	25	90	trace	45	35	48	50	45	55	62	84	53
Clinopyroxene	35	6	5	20	15	25	32	32	28	20	8	20
Magnetite	30	2	92	20	36	20	12	20	15	7	8	12
Olivine	2	2	2	12	4	5	1	1	2	8	0	8
Amphibole	8	trace	1	3	10	2	5	2	trace	1	0	2
Apatite	0	trace	trace	trace	trace	trace	trace	trace	trace	2	0	5
Biotite	0	0	0	0	0	0	0	0	0	0	0	0
Quartz	0	0	0	0	0	0	0	0	0	0	0	0
Titanite	0	tr	0	0	0	0	0	0	0	0	0	0
Epidote	0	0	0	0	0	0	0	0	0	0	0	0

Lithological zone:	Middle Zone									
Sample no.:	Lj-28	Lj-29	Lj-30	Lj-31	Lj-33	Lj-34	Lj-35	Lj-36	Lj-37	Lj-38
Rock name:	Ol Gab	Anorth	Ol Gab	Ol Gab	Ol Gab	Ol Gab	Anorth	Ol Gab	Ol Gab	Gab
Meters above base:	500	550	610	660	780	860	892	915	950	1000
Plagioclase	57	72	46	60	40	45	83	45	52	45
Clinopyroxene	20	2	25	15	25	30	6	30	30	36
Magnetite	12	1	16	13	18	12	5	15	10	15
Olivine	5	0	7	7	8	6	3	5	8	1
Amphibole	2	8	1	1	4	3	0	1	trace	3
Apatite	4	tr	5	4	5	4	3	4	trace	trace
Biotite	0	5	0	0	0	0	0	0	0	0
Quartz	0	12	0	0	0	0	0	0	0	0
Titanite	0	0	0	0	0	0	0	0	0	0
Epidote	0	0	0	0	0	0	0	0	0	0

Table 1: continued

Lithological zone:	Upper Zone										
Sample no.:	Lj-39	Lj-40	Lj-41	Lj-43	Lj-44	Lj-45	Lj-46	Lj-47	Lj-48	Lj-49	P-40
Rock name:	Ol Gab	Anorth	Ol Gab	Gab	Gab	Ol Gab	Ol Gab	Ol Gab	Gab	Gab	Anorth
Meters above base:	1172	1180	1185	1195	1220	1250	1280	1350	1400	1500	1600
Plagioclase	3	99	70	55	70	50	55	45	53	45	86
Clinopyroxene	50	0	20	30	17	35	25	32	30	30	5
Magnetite	28	<1	5	13	10	6	14	13	15	13	1
Olivine	15	0	5	0	0	7	5	7	trace	0	0
Amphibole	3	0	trace	2	3	2	1	3	2	11	0
Apatite	trace	trace	trace	trace	trace	trace	trace	trace	trace	1	trace
Biotite	0	0	0	0	0	0	0	0	0	0	0
Quartz	0	0	0	0	0	0	0	0	0	0	0
Titanite	0	0	0	0	0	0	0	0	0	0	trace
Epidote	0	0	0	0	0	0	0	0	0	0	8

Modes include fresh and altered grains, except for amphibole, which is after clinopyroxene. Ol Gab, olivine gabbro; Gab, gabbro; Ore, magnetite ore; Anorth, anorthosite.

to intrude the underlying marble (Tang, 1984). The ores in these two localities contain the same minerals. The occurrence of the intrusive ore bodies in the marble, which do not show any evidence of skarn origin, was taken as evidence of the existence of oxide magmas (Tang, 1984).

Both massive and disseminated ores are common in the Panzhihua intrusion. The massive ore bodies are planar and always have sharp lower boundaries with the host silicate rocks. In some cases, the massive ores grade upward into disseminated ores, which in turn grade into unmineralized gabbros. The oxide layers are always parallel to the layering in the host rocks and some contain thin intercalations of gabbro. Massive ores typically contain >80% titanomagnetite with variable amounts of clinopyroxene, plagioclase, and olivine. The sparse silicate minerals are completely surrounded by oxides.

Disseminated ores are generally coarse-grained and consist of ~50% titanomagnetite, ~20% clinopyroxene, ~20% plagioclase, ~10% ilmenite, and small amounts of olivine. Most are net-textured, grading to banded or massive with increasing percentages of oxide minerals. The oxide minerals typically partly surround, or enclose, the silicate grains, which may be up 5 mm in diameter (Fig. 4c and d). Clinopyroxene grains in these ores are commonly rimmed with brown hornblende (Fig. 4c). The clinopyroxene contains two sets of exsolution lamellae marked by ilmenite laths oriented parallel to the prismatic cleavage (Fig. 4d).

Both types of oxide ores commonly contain pyrrhotite ranging from 1 modal % in disseminated ores to 5 modal % in massive ores (Fig. 4e–h) and also minor pentlandite. Pyrrhotite occurs as disseminated grains in oxides or as rounded blebs in silicate minerals (Fig. 4e and f). In sample LJ07 a bleb enclosed in clinopyroxene consists of pyrrhotite and magnetite. Pyrrhotite may also show an equilibrium texture with oxide minerals (Fig. 4h).

ANALYTICAL METHODS

SHRIMP zircon analyses

Zircon grains were separated using conventional heavy liquid and magnetic techniques, mounted in epoxy, polished, coated with gold, and photographed in transmitted and reflected light to identify grains for analyses. U–Pb isotopic ratios of zircon separates were measured using the SHRIMP II at Curtin University of Technology in Perth, Western Australia. The measured isotopic ratios were reduced off-line using standard techniques and the U–Pb ages were normalized to a value of 564 Ma determined by conventional U–Pb analysis of zircon standard CZ3. Common Pb was corrected using the methods of Compston *et al.* (1984). The $^{206}Pb/^{238}U$ and $^{207}Pb/^{235}U$ data were corrected for uncertainties associated with the measurements of the CZ3 standard.

Whole-rock geochemical analyses

Samples were collected systematically from a surface section from the bottom to the top of the Lanjian block (Fig. 2). Their modal mineralogy and stratigraphic heights are described in Table 1. Whole-rock samples were cut with a diamond-bonded brass saw blade, crushed in a steel jaw crusher that was cleaned extensively with deionized water between samples, and pulverized in agate mortars in order to minimize potential contamination of transition metals in trace element

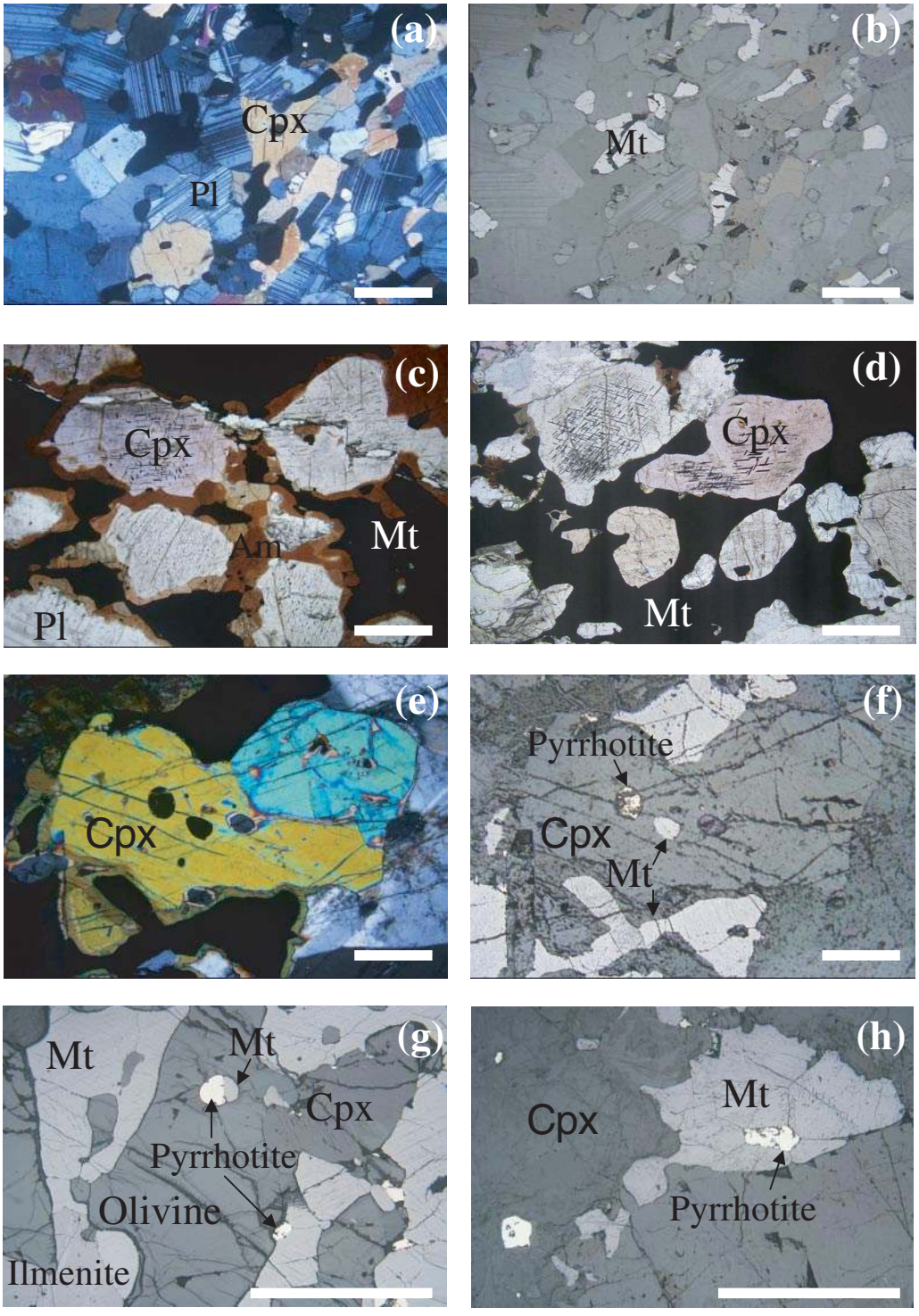

Fig. 4. Photomicrographs of samples from the Panzhihua intrusion, SW China. (a) and (b) a gabbro containing clinopyroxene and plagioclase with disseminated magnetite; sample LJ08. (c) Magnetite (black) enclosing clinopyroxene and plagioclase, both of which are rimmed by brown amphibole, suggesting reaction between the hydrous oxide melt and the silicate minerals; sample P21. (Note also ilmenite exsolution along the clinopyroxene cleavages.) (d) Magnetite completely enclosing rounded clinopyroxene grains showing two sets of exsolution lamellae along the cleavage; sample P28. (e) and (f) rounded blebs of sulfide (pentlandite) and magnetite in clinopyroxene; sample P15. (g) Sulfide–magnetite bleb and disseminated pyrrhotite (white patches); sample LJ06. (h) Equilibrium texture of pentlandite and magnetite and disseminated pyrrhotite; sample LJ07. (a) and (e) were taken under transmitted light with crossed polars; (c) and (d) under plane-polarized light; (b), (f), (g) and (h) under reflected light. Pl, plagioclase; Cpx, clinopyroxene; Am, amphibole; Mt, magnetite. The scale bar is 0.5 mm.

Table 2: SHRIMP zircon analytical data of a leucogabbro (PZH72) from the Panzhihua intrusion, SW China

Spot	Concentration (ppm)			Th/U	%Con.	Ages (Ma)							
	U	Th	Pb			$^{206}Pb/^{238}U$	±	$^{207}Pb/^{235}U$	±	$^{207}Pb/^{206}Pb$	±	$^{208}Pb/^{232}Th$	±
PZH72-1	325	237	15	0·72912	179	259	3	248	12	144	112	251	8
PZH72-2	574	487	28	0·84845	80	270	3	277	4	337	26	268	4
PZH72-3	345	275	16	0·79909	86	259	3	263	9	303	78	258	6
PZH72-4	316	319	15	1·0083	125	261	3	255	10	208	94	265	6
PZH72-5	474	542	24	1·1437	91	264	3	267	7	291	63	264	5
PZH72-6	652	483	30	0·74072	93	262	3	264	4	282	25	262	4
PZH72-7	856	646	39	0·75408	94	260	3	261	4	276	22	259	4
PZH72-8	472	375	23	0·79482	89	270	3	273	4	303	28	270	4
PZH72-9	661	342	29	0·51793	113	262	3	259	6	233	50	254	6
PZH72-10	442	288	20	0·6512	99	265	3	266	7	269	57	270	6
PZH72-11	307	232	14	0·75505	140	261	3	254	10	187	99	256	7
PZH72-12	277	191	13	0·68884	92	265	3	267	9	288	79	258	7
PZH72-13	729	625	34	0·85807	105	261	3	260	6	249	54	259	5
PZH72-14	531	299	23	0·5629	84	257	3	262	6	306	50	260	6
PZH72-15	265	208	12	0·78487	99	259	3	259	5	263	38	260	5

analysis. Major oxides were determined by wavelength-dispersive X-ray fluorescence spectrometry (WD-XRFS) on fused glass disks at The University of Hong Kong. Selected trace elements (Sc, V, Cr, Ni, Cu, and Zn) were determined by WD-XRFS on pressed powder pellets. Other trace elements, including rare earth elements (REE), were analyzed by inductively coupled plasma mass spectrometry (ICP-MS) using a VG Elemental PlasmaQuad Excell system at The University of Hong Kong. Standard additions were used to establish absolute abundances, pure elemental standards were used for external calibration, and BHVO-1 was employed as a reference material. Accuracies of the XRF analyses are estimated to be ±2% (relative) for major oxides present in concentrations >0·5 wt % and ±5% (relative) for trace elements. Accuracies of the ICP-MS analyses are estimated to be better than ±5% (relative). Major oxide and trace element data are given in Table 2.

ANALYTICAL RESULTS

SHRIMP zircon analytical results

Zircon was extracted from a leucogabbro sample, PZH72, from the upper zone of the Panzhihua intrusion. Numerous zircon grains were obtained and all are euhedral and display oscillatory zoning, features indicative of an igneous origin. Fifteen spots on 15 grains were analyzed (Table 2). Excluding two analyses (PZH72-1 and PZH72-14), which have large analytical errors, the analyses yielded $^{206}Pb/^{238}U$ ages of 263 ± 3 Ma and identical $^{207}Pb/^{235}U$ ages of 265 ± 4 Ma within uncertainties (Fig. 5). There is no evidence of overgrowths or inherited cores and the analysed zircons have igneous zoning in CL imagines. Because the $^{206}Pb/^{238}U$ ages reflect crystallization ages if they are younger than 1000 Ma, we consider that 263 ± 3 Ma is the best estimation of the crystallization age of the Panzhihua intrusion.

Major elements

All of the analyzed samples are relatively fresh as observed under the microscope and as indicated by their small loss-on-ignition (LOI) values (Table 3). As expected from their range of modal mineralogy, the rocks exhibit large compositional variations. For example, SiO_2 contents range from 30 to 51 wt % and Al_2O_3 contents from 10 to 24 wt % (Table 3). Na_2O and K_2O range from 1·4 to 4·5 wt % and from 0·01 to 0·45 wt %, respectively, whereas CaO shows a relatively narrow range between 10 and 13 wt %. The gabbros are relatively rich in TiO_2 and Fe_2O_3, ranging between 0·5 and 9·2 wt % and 1·5 and 20 wt %, respectively.

There is no systematic variation of major oxides through the intrusion, although there is a slight overall decrease in MgO and Fe_2O_3 (as total iron) and an increase in SiO_2, Na_2O, Al_2O_3, and CaO upward (Fig. 6). Titanium concentrations are highest in the lowermost part of the Lower zone and decrease upward

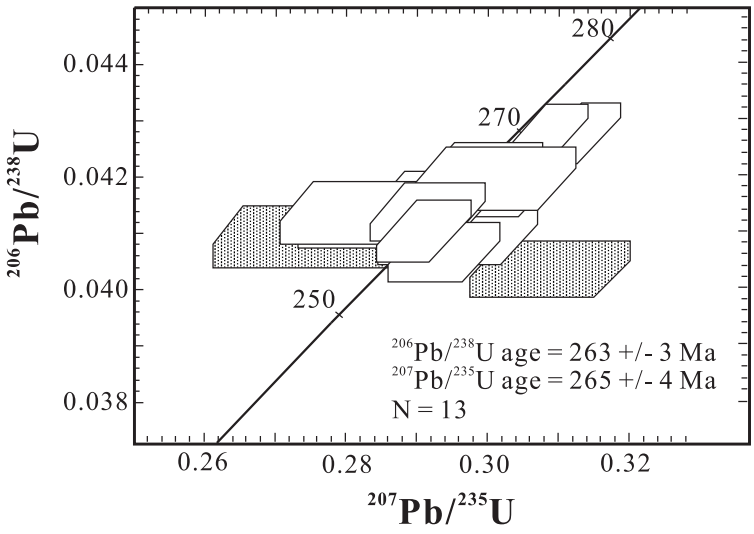

Fig. 5. SHRIMP zircon U–Pb concordia plots of a leucogabbro (PZH72) from the Panzhihua intrusion, SW China. Shaded blocks are analyses that are not included in the age calculation.

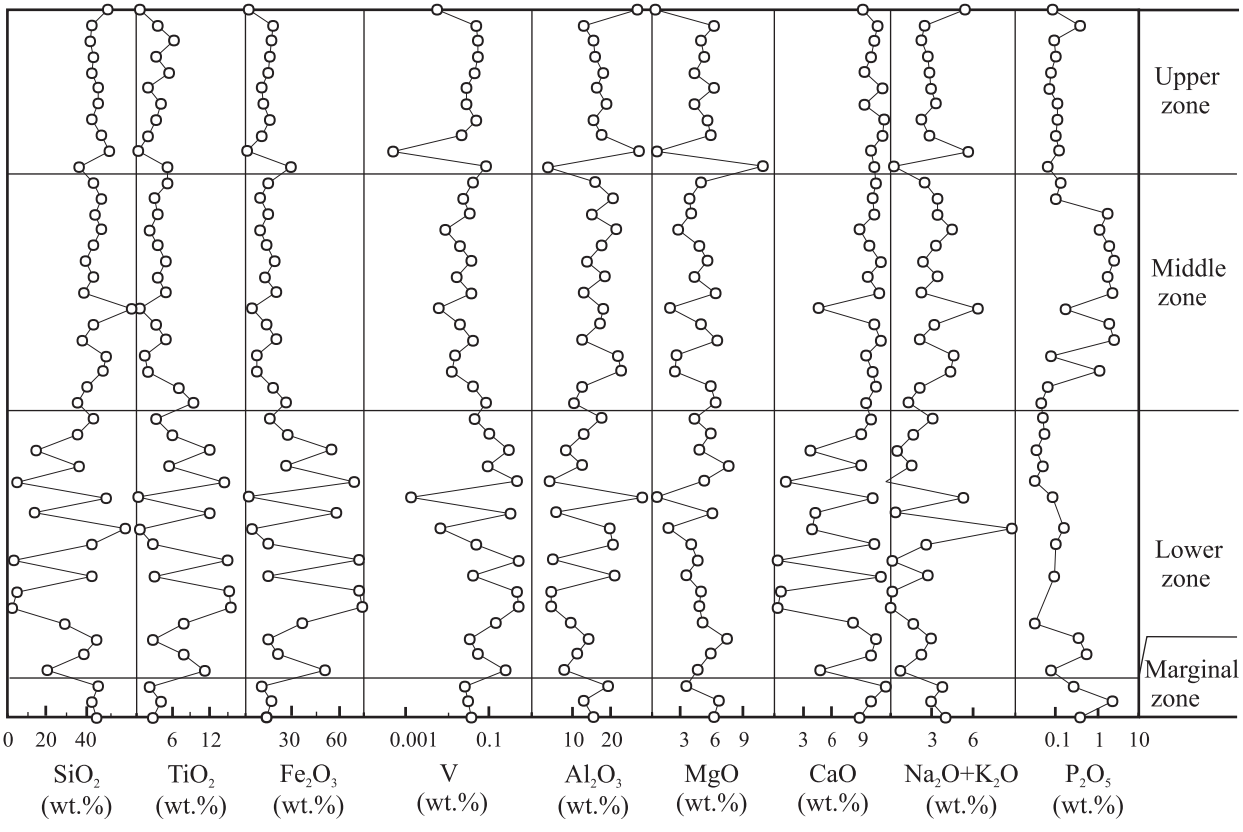

Fig. 6. Chemical variations of major element oxides and trace elements [SiO_2, TiO_2, Fe_2O_3 (as total iron), V, Al_2O_3, MgO, CaO, $Na_2O + K_2O$, and P_2O_5] from the bottom to the top of the Panzhihua intrusion, SW China. It should be noted that the stratigraphic position of each sample is relative and that the four zones are not defined petrologically but based on mining criteria.

through the body (Fig. 6). A number of P-rich horizons occur in the Middle and Lower zones. In the gabbros, Al_2O_3 and total alkalis ($Na_2O + K_2O$) increase with increasing SiO_2, whereas MgO, Fe_2O_3, and TiO_2 decrease (Fig. 7). Fe_2O_3 and TiO_2 are clearly positively correlated and show two slightly different trends (Fig. 8).

On an AFM diagram, the rocks in the Panzhihua intrusion show a tholeiitic Fe-enrichment trend (Fig. 9).

Table 3: Major oxide and trace element concentrations of the Panzhihua intrusion, SW China

	Marginal Zone			Lower Zone					
Sample no.:	LJ-03	LJ-04	LJ-05	LJ-06	LJ-07	LJ-08	LJ-09	LJ-10	LJ-11
Rock name:	Ol Gab	Gab	Gab	Ol Gab	Gab	Gab	Gab	Ore	Ore
Major oxides (wt %)									
SiO_2	44·7	42·1	45·8	19·8	38·6	44·7	29·0	2·03	4·56
TiO_2	2·78	4·09	2·17	11·3	7·73	2·68	7·66	15·5	15·3
Al_2O_3	15·3	12·9	19·2	8·02	11·3	14·2	9·79	5·00	4·86
Fe_2O_3	13·6	16·6	9·9	49·9	20·4	14·2	35·7	74·0	72·3
MnO	0·19	0·27	0·09	0·35	0·27	0·21	0·28	0·38	0·38
MgO	7·16	7·67	3·91	5·16	6·67	8·60	5·78	5·33	5·52
CaO	10·2	11·6	13·4	5·61	11·6	12·2	9·42	0·30	0·87
Na_2O	2·57	2·51	2·88	0·35	1·97	2·30	1·36	0·03	0·06
K_2O	1·41	0·38	0·82	0·35	0·30	0·67	0·25	0·01	0·02
P_2O_5	0·38	2·24	0·27	0·07	0·54	0·34	0·03	0·00	0·00
LOI	1·70	0·49	2·27	0·00	0·55	1·06	0·11	0·00	0·00
Sum	99·96	100·80	100·77	99·76	99·97	101·22	99·45	99·40	99·19
Trace elements (ppm)									
S	122	2114	558	3655	3066	192	11200	8800	10100
Sc	41	38	20	39	57	32	54	85	62
V	373	294	251	2455	538	350	1350	4878	4524
Cr	198	8	6	182	6	315	43	691	950
Ni	55·7	3·6	19·1	77	8·3	132·0	76	169	213·7
Cu	85	32	17	79	52	108	148	263	404
Zn	110	129	49	333	135	117	215	481	474
Sc	29·5	19·5	17·2	27·4	27·9	26·7	36·4	19·4	21·5
Co	48	49	38	147	63	56	125	257	257
Rb	31·5	8·1	12·4	5·4	3·1	9·0	3·7	0·3	0·5
Sr	898	672	1051	259	417	737	331	4	7·5
Y	27·3	38·8	11·1	5·0	21·2	25·8	6·7	0·4	1·0
Zr	138	48	43	35	77	150	22	10	12
Nb	34·0	14·6	5·8	6·1	24·2	35·2	3·3	1·8	2·0
Ba	481	272	467	120	364	494	81	3·2	6·5
La	26·3	28·0	9·9	1·93	11·8	27·8	1·88	0·19	0·46
Ce	60·0	67·0	19·6	4·83	28·1	61·4	5·11	0·44	1·11
Pr	8·26	10·10	2·55	0·75	4·18	8·05	0·89	0·07	0·17
Nd	34·8	48·4	11·2	4·07	20·1	33·4	4·93	0·34	0·88
Sm	7·53	11·48	2·71	1·19	5·20	7·00	1·54	0·09	0·24
Eu	2·60	4·62	1·48	0·62	2·28	2·43	0·86	0·04	0·11
Gd	7·25	11·61	2·83	1·22	5·38	6·69	1·65	0·09	0·25
Tb	1·02	1·58	0·42	0·21	0·80	0·93	0·27	0·02	0·04
Dy	5·59	8·38	2·31	1·16	4·45	5·08	1·53	0·09	0·25
Ho	1·03	1·44	0·41	0·22	0·78	0·93	0·28	0·02	0·04
Er	2·61	3·40	1·03	0·55	1·92	2·44	0·69	0·05	0·11
Tm	0·33	0·38	0·12	0·06	0·23	0·31	0·08	0·00	0·01
Yb	1·95	2·01	0·72	0·40	1·30	1·81	0·48	0·04	0·09
Lu	0·30	0·29	0·11	0·06	0·19	0·28	0·07	0·01	0·01
Hf	3·71	1·43	1·12	1·12	2·11	3·90	0·84	0·43	0·49

	Marginal Zone			Lower Zone					
Sample no.:	LJ-03	LJ-04	LJ-05	LJ-06	LJ-07	LJ-08	LJ-09	LJ-10	LJ-11
Rock name:	Ol Gab	Gab	Gab	Ol Gab	Gab	Gab	Gab	Ore	Ore
Ta	1·74	0·95	0·36	0·45	1·56	1·80	0·25	0·17	0·19
Pb	2·22	0·98	3·10	0·95	2·01	1·87	0·44	12·18	7·87
Th	0·34	0·57	1·68	0·33	0·30	0·76	0·06	0·02	0·04
U	0·12	0·16	0·45	0·16	0·09	0·17	0·02	0·01	0·01
Mg-no.	0·54	0·51	0·47	0·19	0·42	0·57	0·27	0·14	0·15
Cu/Ni	1·54	8·94	0·88	1·03	6·19	0·82	1·95	1·55	1·89

	Lower Zone				Middle Zone			
Sample no.:	LJ-12	LJ-13	LJ-14	LJ-15	LJ-16	LJ-17	LJ-18	LJ-19
Rock name:	Gab	Ore	Gab	Anorth	Gab	Anorth	Ore	Ol Gab
Major oxides (wt %)								
SiO_2	42·8	3·21	42·5	59·2	13·46	49·7	5·02	36·5
TiO_2	2·94	15·1	2·70	0·42	12·2	0·38	14·6	5·24
Al_2O_3	20·6	5·16	20·2	19·6	6·18	27·4	4·37	12·4
Fe_2O_3	14·6	72·1	14·0	4·19	58·0	1·60	68·9	25·6
MnO	0·12	0·37	0·12	0·05	0·33	0·02	0·37	0·22
MgO	3·87	5·24	4·51	1·87	6·97	0·57	5·94	8·71
CaO	12·7	0·47	12·1	4·57	4·86	11·9	1·41	10·4
Na_2O	2·28	0·07	2·27	7·87	0·28	4·43	0·00	1·34
K_2O	0·37	0·02	0·28	0·93	0·02	0·82	0·19	0·16
P_2O_5	0·09	0·00	0·10	0·16	0·00	0·08	0·03	0·05
LOI	0·47	1·89	1·33	1·94	0·00	2·91	0·00	0·00
Sum	100·93	99·71	100·08	100·80	99·51	99·82	98·87	100·14
Trace elements (ppm)								
S	2005	6354	1558	24	7438	589	8535	3546
Sc	32	62	23	10	100	6	79	40
V	414	4843	460	69	3002	13	4528	879
Cr	90	777	107	25	877	2	1136	56
Ni	46·7	272·7	84·8	11·7	146·8	11·2	211·3	46·0
Cu	167	376	198	3	261	77	204	76
Zn	77	466	79	26	355	10	437	144
Sc	7·8	20·0	14·7	12·8	33·0	2·1	23·9	22·8
Co	27	254	50	12	216	10	235	100
Rb	1·5	0·5	6·3	11·5	0·5	5·1	0·2	1·2
Sr	270	10	745	177	57	920	5	336
Y	3·2	0·9	7·6	25·5	3·3	2·4	1·2	6·2
Zr	14	13	41	196	13	12	11	17
Nb	2·0	2·5	5·4	8·2	1·8	2·0	1·8	2·4
Ba	63	8·8	178	1000	9·5	129	2·8	59
La	2·23	0·61	4·96	42·16	0·59	3·01	0·20	1·81
Ce	4·95	1·36	11·45	76·40	1·83	6·13	0·66	4·75

Table 3: continued

	Lower Zone				Middle Zone			
Sample no.:	LJ-12	LJ-13	LJ-14	LJ-15	LJ-16	LJ-17	LJ-18	LJ-19
Rock name:	Gab	Ore	Gab	Anorth	Gab	Anorth	Ore	Ol Gab
Pr	0·67	0·20	1·58	8·26	0·35	0·80	0·13	0·79
Nd	3·02	0·94	7·12	28·78	2·01	3·41	0·74	4·21
Sm	0·74	0·23	1·75	5·12	0·69	0·70	0·26	1·32
Eu	0·45	0·09	0·92	1·28	0·32	0·72	0·11	0·74
Gd	0·78	0·22	1·80	5·15	0·77	0·71	0·29	1·43
Tb	0·12	0·04	0·28	0·73	0·13	0·09	0·05	0·23
Dy	0·65	0·22	1·55	4·22	0·76	0·50	0·28	1·36
Ho	0·11	0·04	0·29	0·85	0·13	0·09	0·05	0·24
Er	0·29	0·10	0·71	2·54	0·34	0·23	0·13	0·58
Tm	0·04	0·01	0·09	0·38	0·04	0·03	0·02	0·07
Yb	0·20	0·07	0·52	2·42	0·24	0·16	0·09	0·38
Lu	0·03	0·01	0·08	0·40	0·04	0·02	0·01	0·06
Hf	0·39	0·49	1·09	5·00	0·60	0·32	0·47	0·64
Ta	0·13	0·22	0·32	0·55	0·16	0·14	0·16	0·20
Pb	0·38	1·44	1·35	11·39	1·47	2·17	0·95	0·86
Th	0·12	0·06	0·44	10·58	0·03	0·21	0·01	0·11
U	0·03	0·02	0·12	2·10	0·01	0·05	0·01	0·02
Mg-no.	0·37	0·14	0·42		0·21		0·16	0·43
Cu/Ni	3·58	1·38	2·34		1·78		0·96	1·65

	Middle Zone								
Sample no.:	LJ-20	LJ-21	LJ-22	LJ-23	LJ-24	LJ-25	LJ-26	LJ-27	LJ-28
Rock name:	Gab	Ol Gab	Gab	Gab	Gab	Ol Gab	Anorth	Ol Gab	Ol Gab
Major oxides (wt %)									
SiO_2	14·7	35·4	43·6	35·0	40·3	48·2	49·9	37·9	43·1
TiO_2	12·2	5·82	3·24	9·29	6·97	1·75	1·38	4·95	3·22
Al_2O_3	8·45	13·0	17·4	10·5	12·4	22·4	21·5	12·5	17·1
Fe_2O_3	54·8	26·9	15·6	25·7	17·6	7·15	7·37	19·6	13·8
MnO	0·33	0·22	0·15	0·24	0·22	0·09	0·08	0·23	0·17
MgO	5·36	6·78	4·84	7·36	6·77	2·64	2·85	7·49	5·51
CaO	4·27	10·5	11·7	11·0	12·3	11·8	11·0	12·9	12·0
Na_2O	0·21	1·48	2·89	1·08	1·77	4·06	4·13	1·92	2·92
K_2O	0·20	0·20	0·18	0·20	0·29	0·23	0·41	0·17	0·19
P_2O_5	0·03	0·05	0·05	0·04	0·06	1·13	0·07	2·59	1·91
LOI	0·00	0·00	0·40	0·00	1·23	0·65	0·76	−0·64	0·06
Sum	98·63	99·85	99·98	99·93	99·95	100·04	99·49	99·58	99·94
Trace elements (ppm)									
S	8591	5056	5129	5805	3087	570	2203	2814	2077
Sc	47	49	29	72	36	10	11	31	12
V	2925	985	441	824	397	124	151	393	199
Cr	318	66	10	18	6	1	−1	11	14
Ni	82·5	41·4	10·5	7·5	4·0	3·8	2·9	0·8	1·5

	Middle Zone								
Sample no.:	LJ-20	LJ-21	LJ-22	LJ-23	LJ-24	LJ-25	LJ-26	LJ-27	LJ-28
Rock name:	Gab	Ol Gab	Gab	Gab	Gab	Ol Gab	Anorth	Ol Gab	Ol Gab
Cu	154	103	29	39	27	5	15	14	12
Zn	357	143	83	126	98	42	40	112	82
Sc	21·5	23·6	19·5	28·8	23·3	5·2	11·0	15·6	12·0
Co	203	100	66	92	55	21	30	60	42
Rb	0·5	1·8	1·5	1·6	3·8	0·9	3·3	0·7	0·9
Sr	154	364	574	352	357	872	757	504	705
Y	2·0	6·6	6·3	7·8	8·6	11·7	5·6	28	22
Zr	12	23	15	25	26	9	14	15	11
Nb	1·9	2·8	2·0	7·3	10·1	2·2	1·6	3·8	2·6
Ba	23	71	114	77	115	152	249	77	110
La	0·57	2·23	2·12	1·40	2·21	8·22	4·66	15·6	13·6
Ce	1·45	5·65	5·21	4·23	5·95	20·9	9·48	43·1	36·2
Pr	0·24	0·90	0·84	0·79	1·04	3·25	1·22	7·00	5·93
Nd	1·44	4·65	4·42	4·64	5·86	16·7	5·42	36·7	30·9
Sm	0·44	1·41	1·32	1·56	1·85	3·94	1·32	9·28	7·49
Eu	0·27	0·77	0·97	0·89	1·12	2·20	1·26	3·39	3·05
Gd	0·46	1·55	1·47	1·79	2·11	4·07	1·44	9·42	7·60
Tb	0·08	0·24	0·24	0·29	0·33	0·52	0·21	1·25	0·98
Dy	0·45	1·41	1·36	1·71	1·88	2·61	1·17	6·16	4·82
Ho	0·08	0·26	0·24	0·30	0·33	0·43	0·21	1·01	0·79
Er	0·21	0·60	0·58	0·72	0·80	0·96	0·51	2·18	1·71
Tm	0·02	0·08	0·07	0·09	0·10	0·10	0·06	0·23	0·17
Yb	0·15	0·40	0·39	0·47	0·52	0·49	0·34	1·09	0·82
Lu	0·02	0·06	0·06	0·07	0·08	0·07	0·05	0·15	0·11
Hf	0·46	0·76	0·53	0·93	0·91	0·29	0·47	0·55	0·37
Ta	0·17	0·20	0·18	0·73	0·84	0·16	0·13	0·31	0·21
Pb	1·62	1·01	0·67	0·19	0·68	0·45	1·54	0·25	0·50
Th	0·02	0·15	0·11	0·03	0·06	0·15	0·25	0·20	0·16
U	0·01	0·04	0·03	0·01	0·03	0·04	0·05	0·05	0·05
Mg-no.	0·18	0·36	0·41	0·39	0·46	0·45	0·46	0·46	0·47
Cu/Ni	1·87	2·48	2·81	5·26	6·66	1·42	5·18	16·68	7·83

	Middle Zone								
Sample no.:	LJ-29	LJ-30	LJ-31	LJ-33	LJ-34	LJ-35	LJ-36	LJ-37	LJ-38
Rock name:	Anorth	Ol Gab	Ol Gab	Ol Gab	Ol Gab	Anorth	Ol Gab	Ol Gab	Gab
Major oxides (wt %)									
SiO_2	62·7	38·5	43·4	39·2	42·9	47·3	44·4	47·6	43·1
TiO_2	0·42	4·83	3·40	4·71	3·58	2·27	3·54	3·00	5·12
Al_2O_3	18·0	13·0	18·2	13·7	17·4	21·2	15·0	20·2	15·9
Fe_2O_3	3·74	19·1	12·7	18·1	13·4	8·83	14·8	9·30	14·3
MnO	0·06	0·23	0·16	0·21	0·18	0·10	0·27	0·12	0·17
MgO	2·05	7·24	4·90	6·40	5·37	2·97	4·41	4·22	5·65

Table 3: continued

	Middle Zone								
Sample no.:	LJ-29	LJ-30	LJ-31	LJ-33	LJ-34	LJ-35	LJ-36	LJ-37	LJ-38
Rock name:	Anorth	Ol Gab	Ol Gab	Ol Gab	Ol Gab	Anorth	Ol Gab	Ol Gab	Gab
CaO	5·3	12·5	11·2	12·9	11·4	10·2	12·0	11·9	12·24
Na_2O	5·86	2·06	3·14	2·12	3·02	4·27	3·23	3·26	2·27
K_2O	0·42	0·18	0·28	0·17	0·21	0·19	0·19	0·17	0·17
P_2O_5	0·16	2·43	1·71	2·45	1·87	1·13	1·82	0·09	0·13
LOI	0·85	0·00	0·39	0·23	0·23	1·00	0·61	0·29	0·53
Sum	99·52	99·76	99·54	100·17	99·56	99·44	100·25	100·20	99·63
Trace elements (ppm)									
S	154	2422	132	2886	1949	993	402	1184	1485
Sc	10	26	11	30	15	7	33	25	39
V	62	369	161	362	191	87	320	236	411
Cr	32	15	7	16	10	59	18	32	12
Ni	13·0	0·2	2·8	1·1	1·8	3·2	20	33	16
Cu	4	14	9	13	9	7	21	37	51
Zn	40	112	78	107	80	53	78	38	52
Sc	10·1	15·1	9·9	15·0	10·9	4·7	28·2	18·6	28·0
Co	10	57	36	54	39	21	25	37	51
Rb	5·3	0·9	2·1	0·8	1·9	0·6	0·7	1·0	1·5
Sr	667	526	798	524	770	961	620	584	477
Y	16·2	27	18	26	23	14	21	4·3	6·3
Zr	142	18	11	14	17	8	9	13	16
Nb	4·2	4·3	3·3	3·6	4·1	2·6	1·3	2·6	3·1
Ba	536	92	142	87	130	140	368	239	213
La	22·82	15·4	12·4	14·9	15·6	11·0	15·0	2·48	2·57
Ce	43·23	41·5	32·9	41·3	40·6	27·5	40·6	5·98	6·70
Pr	4·99	6·84	5·24	6·74	6·40	4·24	6·84	0·93	1·14
Nd	18·39	36·1	27·0	35·2	32·4	21·3	36·0	4·81	6·26
Sm	3·52	8·94	6·52	8·73	7·76	4·96	8·54	1·29	1·80
Eu	1·34	3·39	2·87	3·30	3·08	2·58	4·75	1·13	1·22
Gd	3·42	9·23	6·58	8·97	7·83	5·05	8·57	1·34	1·91
Tb	0·49	1·21	0·84	1·16	1·03	0·65	1·07	0·19	0·28
Dy	2·88	6·03	4·15	5·78	5·13	3·22	5·07	1·01	1·48
Ho	0·57	0·98	0·68	0·96	0·84	0·53	0·81	0·17	0·25
Er	1·59	2·18	1·45	2·12	1·86	1·16	1·78	0·40	0·57
Tm	0·23	0·23	0·14	0·21	0·19	0·12	0·18	0·04	0·07
Yb	1·38	1·09	0·71	1·05	0·91	0·59	0·85	0·24	0·35
Lu	0·22	0·15	0·10	0·15	0·13	0·08	0·12	0·04	0·05
Hf	3·36	0·63	0·35	0·53	0·55	0·25	0·33	0·43	0·58
Ta	0·20	0·35	0·26	0·29	0·32	0·21	0·11	0·19	0·25
Pb	7·10	0·31	0·61	1·42	0·97	0·64	0·40	0·42	2·88
Th	2·70	0·29	0·17	0·22	0·24	0·10	0·13	0·05	0·07
U	0·50	0·07	0·05	0·06	0·07	0·03	0·05	0·01	0·02
Mg-no.		0·46	0·46	0·44	0·47	0·43	0·40	0·50	0·47
Cu/Ni		81·93	3·36	12·52	4·86	2·14	1·06	1·12	3·15

	Upper Zone										
Sample no.:	LJ-39	LJ-40	LJ-41	LJ-43	LJ-44	LJ-45	LJ-46	LJ-47	LJ-48	LJ-49	P-40
Rock name:	Ol Gab	Anorth	Ol Gab	Gab	Gab	Ol Gab	Ol Gab	Ol Gab	Gab	Gab	Anorth
Major oxides (wt %)											
SiO_2	36·3	51·2	47·5	42·7	45·8	45·8	42·4	43·2	41·4	42·8	50·2
TiO_2	5·21	0·21	1·83	3·12	3·98	1·98	5·31	3·32	6·14	3·41	0·48
Al_2O_3	3·9	26·7	17·4	15·2	18·8	16·2	17·8	15·9	15·3	12·9	26·5
Fe_2O_3	28·7	0·94	10·2	15·7	11·1	10·6	14·7	15·5	16·2	17·5	1·86
MnO	0·36	0·01	0·15	0·16	0·13	0·14	0·14	0·17	0·16	0·24	0·02
MgO	12·7	0·49	6·72	6·32	4·79	7·01	4·90	5·93	5·68	7·15	0·36
CaO	12·1	11·6	13·0	13·2	10·8	13·0	10·9	11·6	12·1	12·4	10·6
Na_2O	0·16	4·51	2·65	1·95	2·98	2·53	2·44	2·41	1·99	2·05	4·69
K_2O	0·08	1·11	0·13	0·22	0·29	0·37	0·32	0·34	0·18	0·46	0·71
P_2O_5	0·06	0·11	0·10	0·10	0·11	0·07	0·07	0·10	0·09	0·37	0·08
LOI	0·59	2·81	0·44	0·66	1·15	2·22	0·63	1·36	0·58	0·68	2·93
Sum	100·12	99·75	100·09	99·40	99·98	99·77	99·60	99·77	99·76	99·97	98·45
Trace elements (ppm)											
S	311	41	−27	1583	369	1034	2050	1401	2453	1437	
Sc	94	4	33	32	25	31	29	28	47	52	20
V	827	5	218	494	291	276	450	506	527	497	58
Cr	857	3	286	236	1	225	15	128	11	66	
Ni	19	6·7	85	194	28	97	26	108	56	89	4·6
Cu	73	10	115	325	39	216	69	253	76	198	
Zn	125	4	43	70	40	44	46	55	49	105	10
Sc	47·3	1·4	24·9	30·2	18·7	27·6	23·1	27·2	31·0	28·6	1·1
Co	72	3	37	54	41	44	61	58	64	56	
Rb	0·3	11·3	0·7	2·2	6·3	6·3	5·1	5·8	1·8	7·2	8·7
Sr	56	981	492	415	603	465	512	437	410	416	1105
Y	8·6	1·3	5·7	6·6	4·8	5·5	3·8	5·7	5·1	23·8	1·4
Zr	13	3	10	12	15	9	12	13	12	50	6
Nb	1·1	0·4	1·0	0·9	2·8	0·6	2·7	1·2	2·5	8·8	1·5
Ba	29	577	191	211	233	248	274	273	186	262	216
La	1·42	2·25	2·15	2·06	3·23	1·70	1·55	1·99	1·61	9·64	2·33
Ce	5·09	4·55	5·68	5·74	7·34	4·73	3·97	5·48	4·50	25·06	5·68
Pr	1·06	0·63	0·98	1·04	1·07	0·86	0·68	0·96	0·80	3·92	0·67
Nd	6·64	2·80	5·53	5·95	5·21	5·02	3·64	5·34	4·64	19·11	3·06
Sm	2·26	0·56	1·61	1·81	1·34	1·54	1·09	1·59	1·45	5·15	0·62
Eu	1·09	1·00	1·19	1·18	1·01	1·14	0·94	1·10	1·05	2·22	0·80
Gd	2·46	0·50	1·69	1·97	1·38	1·67	1·15	1·69	1·54	5·43	0·54
Tb	0·36	0·06	0·24	0·29	0·20	0·24	0·17	0·24	0·22	0·85	0·06
Dy	1·97	0·28	1·31	1·50	1·06	1·28	0·88	1·31	1·19	4·80	0·35
Ho	0·33	0·05	0·22	0·25	0·18	0·22	0·15	0·22	0·19	0·88	0·06
Er	0·77	0·11	0·49	0·59	0·42	0·49	0·34	0·50	0·44	2·19	0·15
Tm	0·08	0·01	0·05	0·07	0·05	0·05	0·04	0·06	0·05	0·28	0·02
Yb	0·45	0·06	0·30	0·34	0·29	0·29	0·20	0·32	0·27	1·53	0·11
Lu	0·07	0·01	0·04	0·05	0·04	0·04	0·03	0·05	0·04	0·23	0·01
Hf	0·55	0·07	0·36	0·48	0·47	0·35	0·40	0·45	0·45	1·63	0·20

Table 3: continued

	Upper Zone										
Sample no.:	LJ-39	LJ-40	LJ-41	LJ-43	LJ-44	LJ-45	LJ-46	LJ-47	LJ-48	LJ-49	P-40
Rock name:	Ol Gab	Anorth	Ol Gab	Gab	Gab	Ol Gab	Ol Gab	Ol Gab	Gab	Gab	Anorth
Ta	0·09	0·03	0·07	0·07	0·22	0·05	0·23	0·09	0·22	0·46	0·37
Pb	0·18	0·47	0·51	1·35	1·07	1·08	0·78	1·03	0·63	1·86	2·61
Th	0·03	0·04	0·05	0·05	0·40	0·03	0·03	0·08	0·04	0·18	0·14
U	0·01	0·01	0·01	0·01	0·08	0·01	0·01	0·02	0·01	0·05	0·06
Mg-no.	0·50		0·60	0·47	0·49	0·60	0·43	0·46	0·44	0·48	
Cu/Ni	3·79		1·35	1·68	1·38	2·23	2·60	2·34	1·36	2·23	

Ol Gab, olivine gabbro; Gab, gabbro; Ore, magnetite ore; Anorth, anorthosite; LOI, loss on ignition.

On a MgO–(Al_2O_3 + CaO)–(FeO_{total} + TiO_2) diagram, all of the Panzhihua rocks are richer in Fe and Ti, but poorer in MgO than normal gabbroic rocks (Fig. 10).

Trace elements

The concentrations of V, Ni, and Zr vary widely, ranging from 30 to 680 ppm, 5 to 180 ppm, and 5 to 200 ppm, respectively. Early-formed cumulate rocks, such as olivine gabbro, are rich in both V and Ni. Vanadium is strongly partitioned into titanomagnetite and shows a positive correlation with TiO_2 (Fig. 8). Vanadium is concentrated in the lowermost parts of the Lower and Middle zones, which are ore-bearing gabbros and melanogabbros, but it decreases slightly upward through the intrusion (Fig. 6). Strontium ranges from 50 to 1350 ppm and is concentrated in late-stage cumulate rocks. Scandium shows very little variation, ranging from 40 to 50 ppm; Sc contents are generally believed to be controlled by clinopyroxene crystallization (e.g. Rollison, 1993), but these rocks show no correlation between Sc contents and the modal abundance of clinopyroxene. There are broadly positive correlations between P_2O_5, La, and total REE (Fig. 11). Zirconium and Nb also show a positive correlation (Fig. 11).

Most of the samples are enriched in light REE (LREE) relative to heavy REE (HREE) and show small positive Eu anomalies (Fig. 12). The oxide ores have low total REE and relatively flat chondrite-normalized REE patterns, whereas the gabbros have higher REE contents and more LREE-enriched/HREE-depleted patterns. Except for anorthosites, all of the rocks in the Panzhihua intrusion are enriched in Ti relative to elements with similar compatibilities, and do not have Nb and Ta anomalies (Fig. 13). The oxide ores have obviously positive Nb and Ta anomalies (Fig. 13). In contrast, U, Th, Zr, and Hf are depleted relative to elements with similar compatibilities.

The Panzhihua magnetite ores have Cu contents ranging from 80 to 404 ppm with an average of 236 ppm, much higher than Ni contents (76–272 ppm and 156 ppm on average). The gabbroic rocks also have variable Cu (5–325 ppm and 78 ppm on average) and Ni contents (0·8–194 ppm and 39 ppm on average). The Cu/Ni ratios of the ores and gabbroic rocks are in the range of 0·96–1·95 (average 1·6) and 0·82–17 (average 3·8), respectively (Table 3).

DISCUSSION

Parental magma composition

The parental magma composition(s) at Panzhihua is difficult to estimate, because the marginal zone has been extensively modified by interaction of the magmas with the wall-rocks. The Panzhihua intrusion displays strong Fe enrichment in terms of its chemistry compared with normal gabbros (Figs 9 and 10). The bulk composition of the intrusion, calculated by weighting the average chemical compositions of each zone according to its outcrop area, yields a composition that is considerably richer in Fe and Ti and poorer in Si than normal tholeiitic magmas (Table 4). If the oxide ore bodies are included, the entire intrusion would be even richer in Fe and Ti and poorer in Si. In addition, the presence of ilmenite exsolution lamellae in clinopyroxene in the Panzhihua intrusion (Fig. 4) indicates that the pyroxene crystallized from a Ti-rich melt. The enrichment of Fe and Ti in all of the rocks of the Panzhihua intrusion and the presence of Ti-rich clinopyroxene are indicative of Fe- and Ti-rich parental magmas.

The Fe–Ti-rich gabbros are far too abundant and contain far too much Fe and Ti to be mass balanced

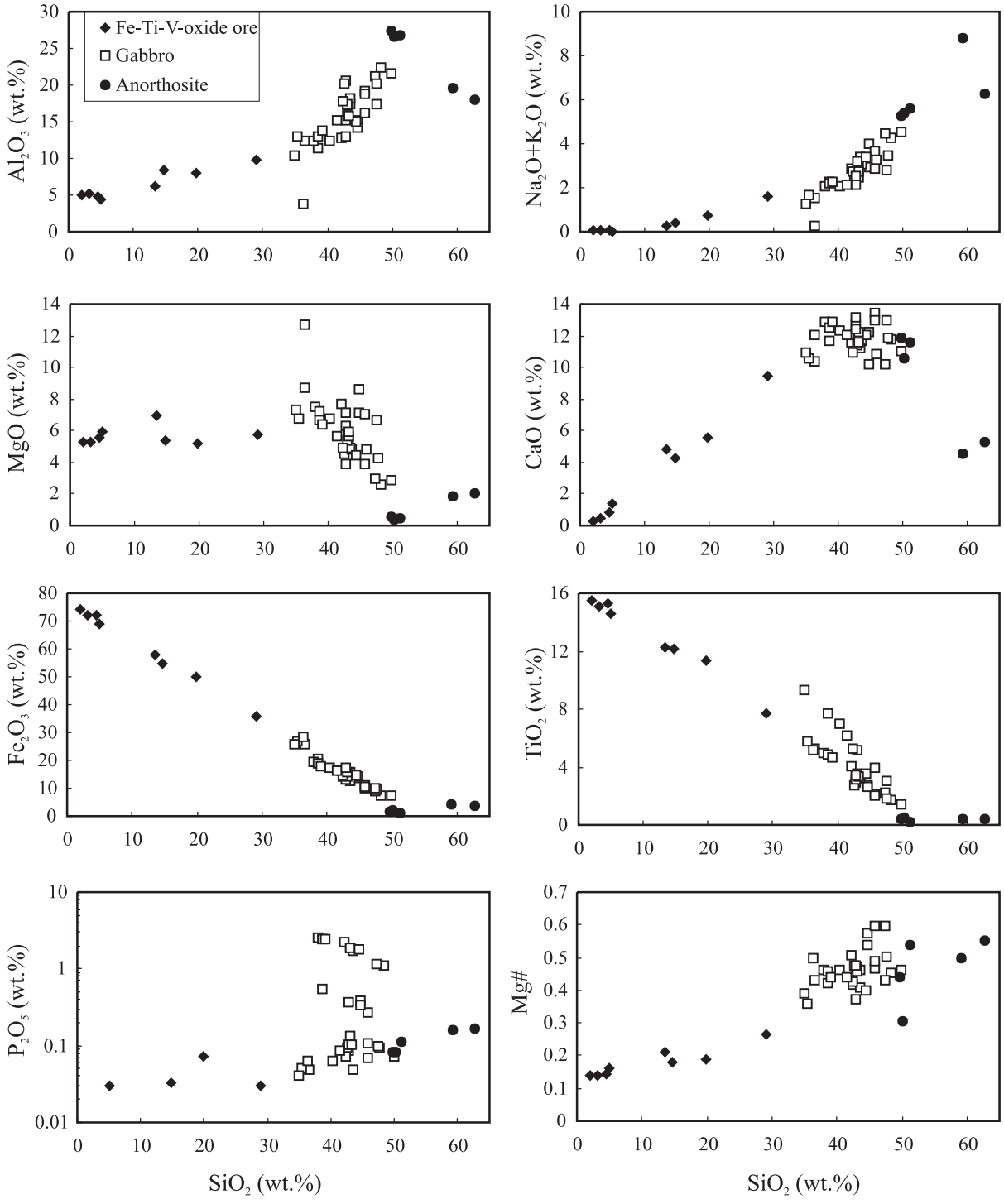

Fig. 7. SiO_2 vs Al_2O_3, $Na_2O + K_2O$, MgO, CaO, Fe_2O_3 (as total iron), TiO_2, P_2O_5 and Mg-number for rocks of the Panzhihua intrusion, SW China.

with any reasonable parental liquid, leaving the possibility that the Fe–Ti-rich magmas must have formed beneath or adjacent to the Panzhihua intrusion and migrated into the Panzhihua magma chamber. There are several explanations for the origin of these high-Fe magmas. It is possible that the Fe enrichment may be a primary feature of the parental magma attributable either to the mantle source composition or conditions of

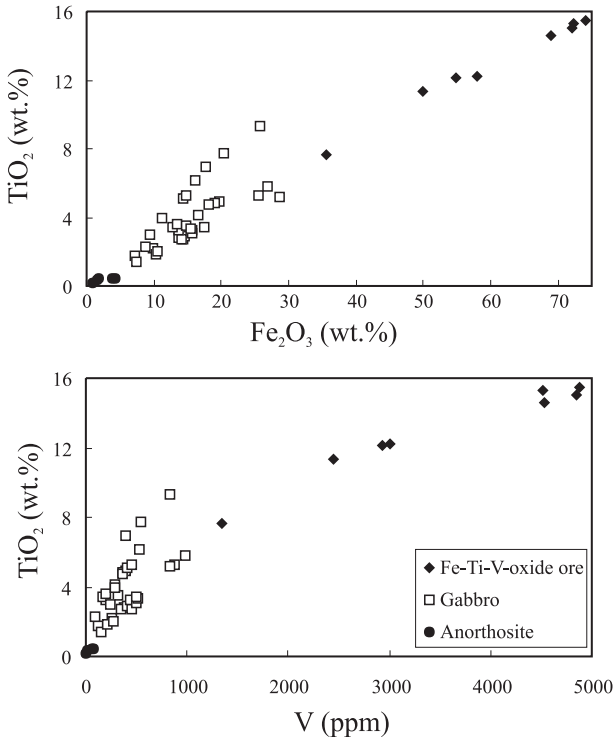

Fig. 8. TiO_2 vs Fe_2O_3 (as total iron) and V in the Panzhihua intrusion, SW China.

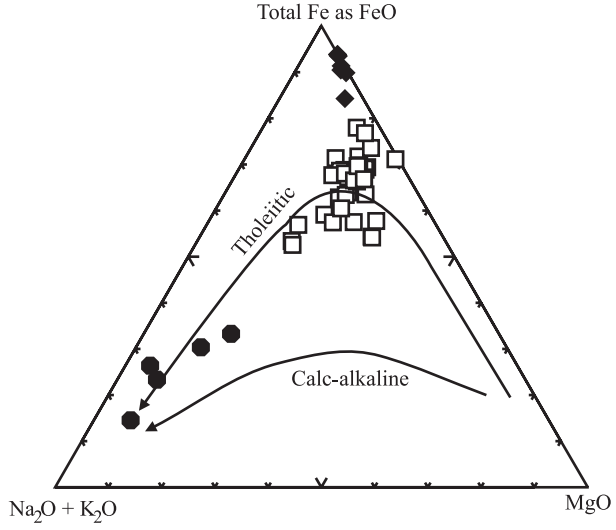

Fig. 9. AFM diagram showing geochemical variations in the Panzhihua intrusion, SW China. The tholeiitic and calc-alkaline trends are after Wilson (1989). Symbols as in Fig. 7.

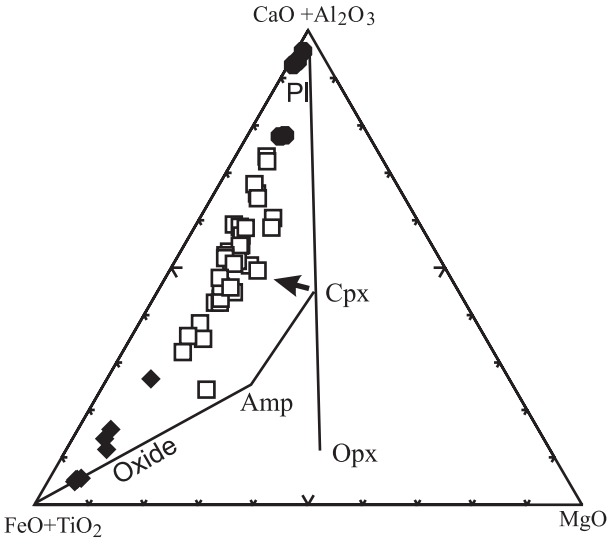

Fig. 10. ($CaO + Al_2O_3$)–($FeO_{total} + TiO_2$)–MgO plot of the Panzhihua intrusion, SW China. Mineral phases plagioclase (Pl), clinopyroxene (Cpx), orthopyroxene (Opx), amphibole (Amp) and oxide are also plotted in this diagram. The arrow indicates the Fe enrichment of rocks from Panzhihua in comparison with the normal gabbros, which should follow the line between plagioclase and clinopyroxene. Symbols as in Fig. 7.

partial melting. However, it is difficult to envision how such dense, high-Fe magmas could migrate from the mantle into the lower crust. A second possibility is that the enrichment resulted from assimilation of Fe-rich rocks, such as banded iron formation, by a normal basaltic magma produced by partial melting of a mantle source. However, there is no evidence of such Fe-rich rocks in the region. A more likely mechanism is that the high-Fe liquids formed through fractionation and thus were highly evolved magmas.

It is known that fractional crystallization of phases such as olivine, clinopyroxene and plagioclase can result in Fe enrichment in the residual liquids (e.g. Hanski, 1992). The Panzhihua rocks are similar to those of late-stage cumulates of the Skaergaard and Kiglapait intrusions (Morse, 1980). Intrusion of Fe-enriched, relatively Si-poor melts has been proposed to explain the upper part of the Skaergaard intrusion, although this suggestion is controversial (see Hunter & Sparks, 1987; Brooks *et al.*, 1991). In the Skaergaard intrusion, tholeiitic magmas appear to have evolved into Fe-enriched, relatively Si-poor products (i.e. Fenner trend) (see Brooks *et al.*, 1991).

The magnetite ores and gabbroic rocks in Panzhihua are relatively rich in Cu, resulting in high Cu/Ni ratios (average 1·8) (Table 3), a feature characteristic of high degrees of fractionation (Lesher & Stone, 1996; Lesher & Keays, 2002). The depletion of Ni relative to Cu can be explained by fractionation of olivine, which preferentially concentrates Ni (Barnes *et al.*, 1985; Keays, 1995). Our unpublished PGE data show very high Pd/Ir ratios (14–24) in Panzhihua, which is again a signature of highly evolved magmas (Keays, 1995). These features, together with very low Mg-number, low Cr and Co contents (Table 3), and LREE enrichment (Fig. 12), are consistent with the parental magmas of Panzhihua being highly evolved.

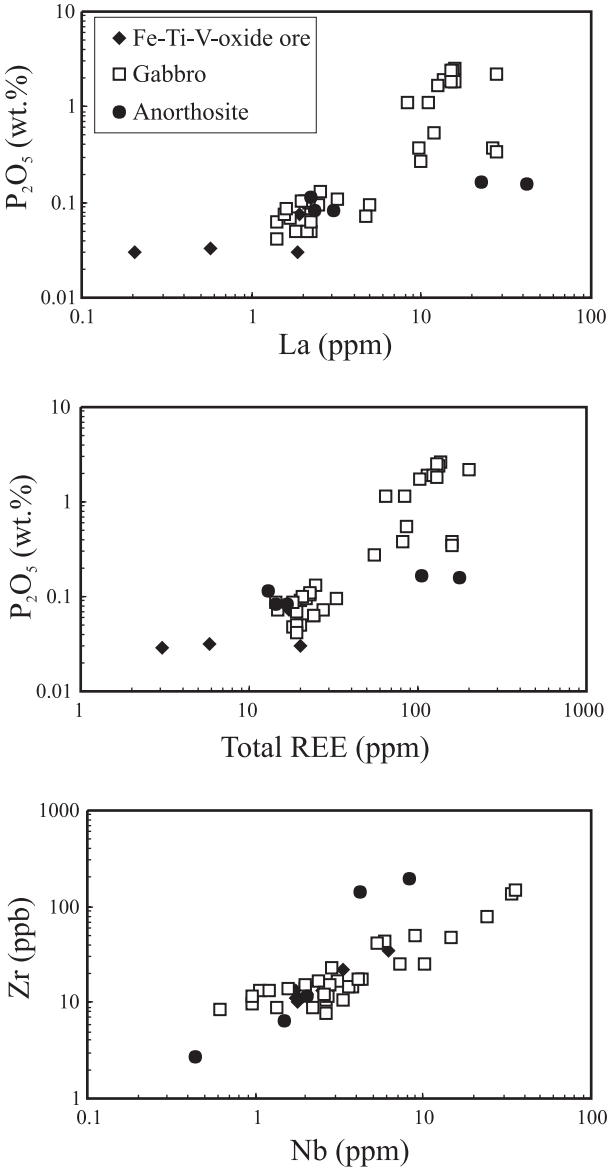

Fig. 11. Trace element relationships of the Panzhihua intrusion, SW China: P_2O_5 vs La, total REE vs P_2O_5, and Nb vs Zr.

A very similar sequence of gabbros containing massive Fe–Ti oxide layers is present in the Atlantis Bank on the flank of the Southwest Indian Ridge in the Indian Ocean and was sampled in Ocean Drilling Program Hole 735B (Robinson *et al.*, 2000; Hertogen *et al.*, 2002). The Fe- and Ti-rich gabbros are concentrated in the upper part of the sequence where they are associated with numerous felsic veins and segregations. The calculated parental magmas for the Hole 735B gabbros have been attributed to an earlier stage of fractionation that would have produced primitive cumulates (Robinson *et al.*, 2000; Hertogen *et al.*, 2002). The calculated melt compositions are highly differentiated ferrobasalt liquids with Mg-numbers generally between 0·35 and 0·6 (Table 4). Fe-rich lavas have also been reported from several other mid-ocean ridges (Table 4) (Ludden *et al.*, 1980; Melson & O'Hearn, 1986). Ferrogabbros and ferropicrites have also been reported from several localities on land where they are considered to have crystallized from evolved Fe-rich liquids (Wiebe, 1979, 1997; Hanksi, 1992). The average composition of the Panzhihua intrusion is comparable with these ferrobasalts and ferropicrites (Table 4). The ferrobasaltic or ferropicritic parental magmas of the Panzhihua intrusion may have formed by crystal fractionation at depth not far from the Panzhihua magma chamber. However, where, why and how this fractionation occurred is not clear.

Source

The Panzhihua intrusion has a crystallization age of ~260 Ma based on SHRIMP zircon analyses (Fig. 5), identical to that of other intrusions within the ELIP (Zhou *et al.*, 2002*c*). It has been documented that the Emeishan flood basalts formed from a Permian mantle plume that reached the base of the lithosphere beneath South China at ~260 Ma (Chung & Jahn, 1995; Song *et al.*, 2001; Xu *et al.*, 2001; Zhou *et al.*, 2002*c*). Geochemically, the Emeishan flood basalts formed from melts derived from an asthenospheric source and modified by an enriched lithospheric component, similar to the source for ocean island basalt (OIB) (Song *et al.*, 2001).

The positive Ti anomalies and negative U, Th, Zr, and Hf anomalies in the Panzhihua rocks (Fig. 13) cannot be explained by upper crustal contamination because upper crustal rocks are typically enriched in these elements and depleted in Nb, Ta, and Ti (Taylor & McLennan, 1985). The Th/U ratios of the Panzhihua rocks vary from 3·0 to 4·0 with an average of 3·5, comparable with ratios of 3·5–3·8 for OIB, but less than ratios of 4·5–4·9 for enriched mantle (EMI) (Weaver, 1990). Zr/Nb ratios in mafic rocks range from about 40 in mid-ocean ridge basalt (MORB) to 10 in E-type MORB, and to <10 in OIB and rift-related lavas (Pearce & Norry, 1979). The Zr/Nb ratios of the Panzhihua gabbros vary between 3 and 15 with most less than 10, again comparable with OIB and the Emeishan flood basalts (Song *et al.*, 2001). Thus, the Panzhihua intrusion appears to have been derived from a slightly enriched asthenospheric melt at ~260 Ma, presumably generated by the same mantle plume that formed the Emeishan flood basalts.

Emplacement, crystallization history and differentiation

The Panxi area has experienced multiple stages of tectonic deformation and the Panzhihua intrusion may have been uplifted during exhumation of associated metamorphic core complexes at ~170 Ma (Zhou *et al.*,

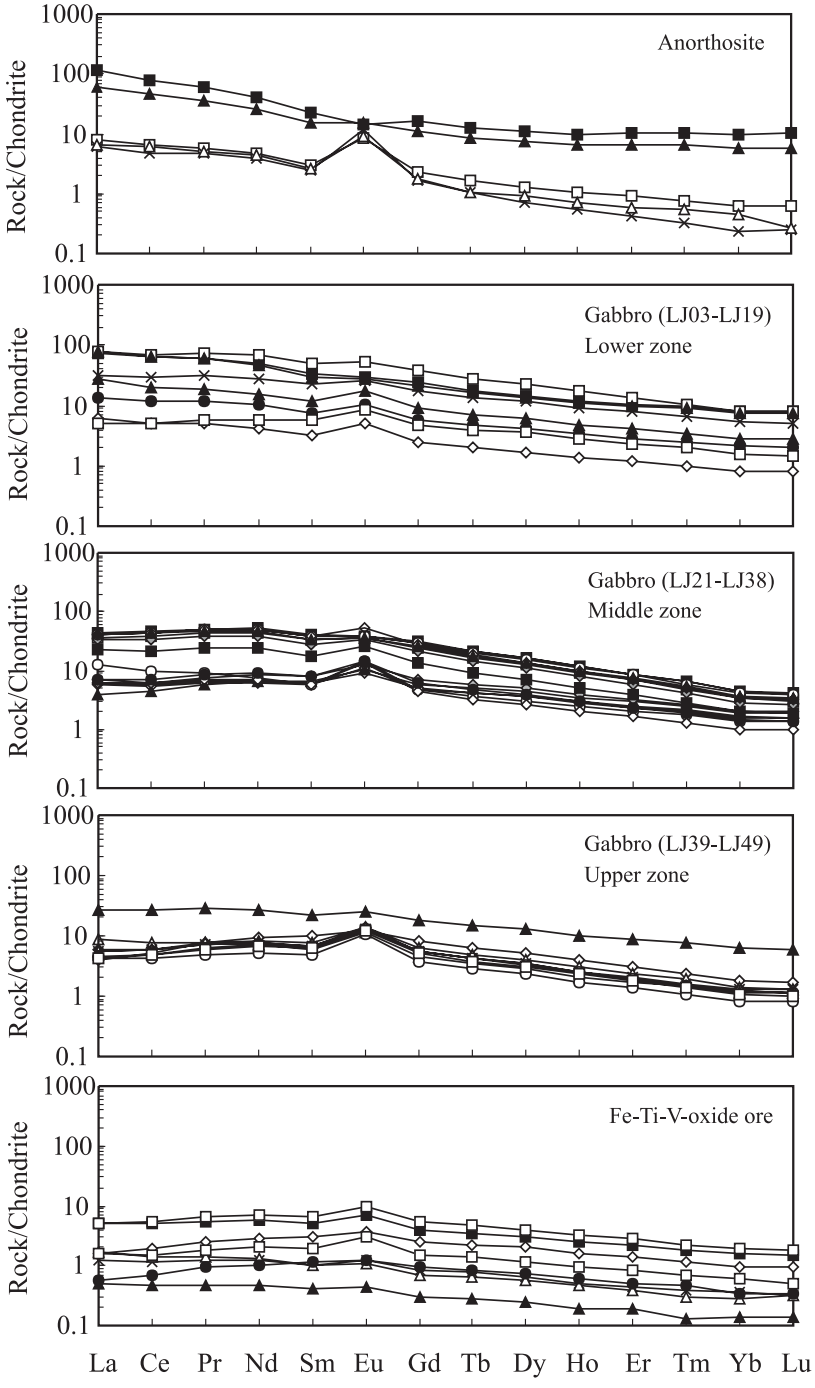

Fig. 12. Chondrite-normalized REE patterns of the Panzhihua intrusion, SW China.

2002*b*; Yan *et al.*, 2003). The intrusive contact between the marginal zone and the underlying contact metamorphosed limestones suggests that the lower part of the intrusion is intact. On the other hand, the top of the body is in fault contact with Permian basalts and Triassic sedimentary rocks, which means that a portion of the upper part has been tectonically removed. Thus, it is possible that the Panzhihua gabbroic body may have been part of a much larger layered intrusion. However, the Panzhihua intrusion is similar in lithology and chemistry to other intact oxide-bearing intrusions, such as the Hongge, Baima, and Xinjie intrusions in nearby areas (Tang, 1984; Zhang *et al.*, 1988; Zhong *et al.*, 2002), indicating that it is relatively complete.

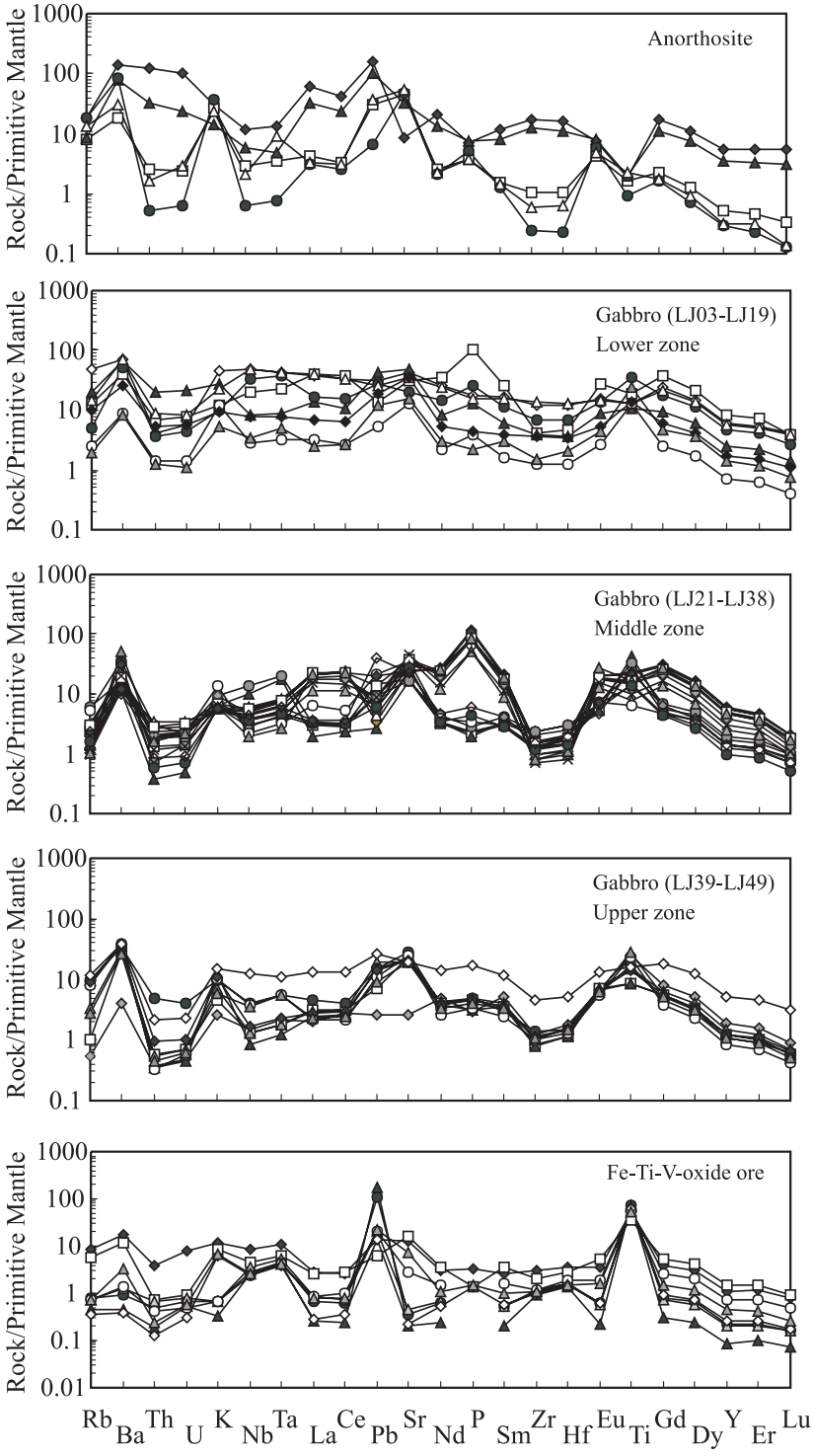

Fig. 13. Primitive mantle normalized trace element diagrams of different units of the Panzhihua gabbroic intrusion. Primitive mantle normalization values are from Sun & McDonough (1989).

Petrographic and geochemical data suggest that the differentiation of the gabbroic body can be accounted for by *in situ*, low-pressure crystallization. The different gabbroic rocks represent mixtures of cumulus phases and trapped liquids, whereas the anorthositic rocks represent derivative liquids.

The banded nature and rhythmic layering of the Panzhihua body are similar to many other layered

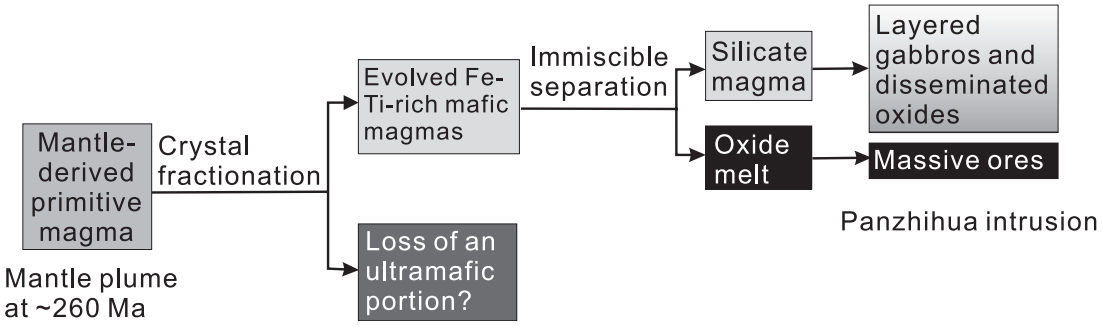

Fig. 14. A schematic model for magma evolution and the formation of the oxide ore deposits in the Panzhihua gabbroic intrusion, SW China.

Table 4: Average composition of the Panzhihua intrusion and other high-Fe mafic magmas

	Panzhihua	Reykjanes Ridge		Skaergaard				EG lava	Galapagos	Hole 735B	Pechenga
		1	2	A	B	D	E				
SiO_2	42·6	49·5	45·3	49·6	48·5	48·5	45·9	47·9	51·2	46·6	46·5
TiO_2	3·99	0·85	5·34	1·39	1·77	4·41	5·51	4·4	3·97	2·97	2·29
Al_2O_3	15·8	16·0	11·6	15·8	14·8	12·6	12·1	12·5	10·1	12·2	10·1
FeO	15·6	9·0	17·4	9·1	11·1	14·9	16·6	15·9	18·4	18·0	15·6
MgO	5·99	9·86	4·58	8·28	7·51	5·86	5·28	5·49	3·92	9·99	14·8
CaO	11·9	12·4	10·4	13·2	11·8	9·4	10·2	10·0	8·74	3·28	8·62
Na_2O	2·45	2·07	2·85	2·13	2·33	2·62	2·65	2·72	2·63	0·1	0·4
K_2O	0·31	0·17	0·62	0·25	0·31	0·59	0·74	0·64	0·29	0·1	1·03
P_2O_5	0·69	0·09	0·42	0·16	0·19	0·36	0·78	0·45	0·47	0·86	0·21
Total	99·2	100·0	98·4	99·8	98·3	99·2	99·7	100·0	99·7	100·0	100·0
Mg-no.	0·46	0·69	0·36	0·65	0·58	0·44	0·39	0·41	0·30	0·35–0·60	0·66

Data sources: Reykjanes Ridge: 1, glass representing mantle-derived melt parental to MORB (Melson & O'Hearn, 1986); 2, glass representative of late liquids in a MOR closed system magma chamber (Melson & O'Hearn, 1986). Skaergaard A–E: successive liquids as suggested by the dykes (Brooks & Nielsen, 1978). EG lava, Tertiary ferrotholeiite from East Greenland (Larsen *et al.*, 1989). Galapagos, microprobe analyses of glass (Fornari *et al.*, 1983). Hole 735B, from Robinson *et al.* (2000) and Hertogen *et al.* (2002). Pechenga, average of ferropicrites in Pechenga, Finland (Hanski, 1992).

mafic–ultramafic intrusions (e.g. Cawthorn, 1996). In the Panzhihua intrusion, crystallization began with olivine, followed by clinopyroxene and plagioclase, and finished with amphibole, titanomagnetite, and sulfide. Thus, the residual melts appear to have been enriched in volatiles and Fe–Ti–V after crystallization of the gabbros. The intercumulus liquids subsequently crystallized, filling the interstices with titanomagnetite (Fig. 4a and b). Early-formed, relatively dense minerals such as olivine may have settled under the influence of gravity to form individual layers.

Mass balance, system dynamics and system size

The formation of igneous layering may involve several mechanisms (e.g. Parsons, 1987; Cawthorn, 1996). One mechanism involves the formation of rhythmic layers by crystallization and mixing of double-diffusive layers in the magma chamber (e.g. Irvine *et al.*, 1983). If this process occurred in the Panzhihua intrusion, it suggests that multiple pulses of magma were injected into the chamber. This model would explain the abundance of leucogabbro in the Upper zone and the predominance of less evolved melanogabbro in the Lower zone.

Although the layering in the body appears to require periodic magma replenishment, this may have occurred in a system that was not erupting, where each influx of magma inflated the chamber. Alternatively, it may have occurred in an open system, in which the magma chamber was tapped during or after it was periodically replenished, or in some combination of the two end-member scenarios. If the composition of the magma influxes remained constant, these processes can be tested by

comparing the integrated bulk composition of the intrusion with the inferred parental magma composition. If they are similar, then the system was not being tapped, but if the intrusion is enriched in cumulus components, the system was open to eruption to some degree, the amount of which can be estimated by mass balance calculation (Table 4). It should be noted that this cannot be tested by examining the major and trace element variations in each cycle, which could be consistent with fractional crystallization in both cases.

Origin of the Fe–Ti–V oxide ores

As a result of very extensive fractionation, magmas in the Skaergaard intrusion, Greenland, evolved into Fe-rich melts, which eventually became FeO saturated, and as a result formed the Fe–Ti–V-oxide-rich rocks of the Triple Group (e.g. Wager & Brown, 1968). Fractionation also produced Fe-rich melts in the Bushveld (South Africa) and Windimura (Western Australia) complexes, which then produced magnetite layers in the upper zones of these complexes, as well as Fe-rich pegmatites in the case of the Bushveld complex (Reynolds, 1985*a*, 1985*b*; Park & Hill, 1986; Scoon & Mitchell, 1994). In the Muskox intrusion, 5–10% magnetite and ilmenite occur in the uppermost gabbro (Irvine, 1988).

Like the Panzhihua intrusion, some intrusions may have been derived from Fe-rich tholeiitic magmas, for example, the Ushushwana and Rooiwater complexes in South Africa. These intrusions do not contain chromitite, but do contain thick ilmenite-rich V-magnetite layers (Winter, 1965; Reynolds, 1978).

The formation of Fe–Ti–(V) oxide ores can be attributed to several different processes. Precipitation of V-bearing titanomagnetite from silicate magmas depends largely on the Fe_2O_3/FeO ratio of the liquid, which is, in turn, a function of the fO_2, temperature, and water content of the magma (e.g. Reynolds, 1985*a*). Crystallization of FeO-bearing phases such as ilmenite, olivine, and pyroxene increases the Fe_2O_3/FeO content of the magma, whereas crystallization of Fe-poor phases such as plagioclase increases the overall Fe content of the magma, and crystallization of all of these anhydrous phases increases the H_2O content. Thus, fractional crystallization of mafic–intermediate magma eventually leads to saturation in Fe_2O_3-bearing phases, first chromite and later magnetite (e.g. Irvine, 1975; Wilson, 1989). An increase in fO_2 and normal fractional crystallization can explain the formation of disseminated, interstitial magnetite (Fig. 4a and b).

Early fractionation of chromite from mafic magmas has formed stratiform chromitite deposits in many layered intrusions. Precipitation of massive chromite layers in such bodies may reflect mixing of evolved and primitive magmas across a cotectic, leading to oversaturation and crystallization of chromite (Irvine, 1975, 1977) and/or contamination of the melt by roof rocks (Kinnaird *et al.*, 2002). This process does not explain the occurrence of magnetite ores in the lower part of the Panzhihua intrusion, because the magnetite in those rocks crystallized later than the silicate minerals (Fig. 4).

Most of the magnetite in the Panzhihua intrusion fills spaces between, or completely encloses, the silicate minerals (Fig. 4). These textural relationships support the case for invasion of dense, Fe-rich melts into a silicate crystal mush (Reynolds, 1985*a*). There are several possible mechanisms by which such a melt could have formed. Crystallization of plagioclase can lead to a dense residual liquid with high total Fe content, which would tend to accumulate as a stagnant layer on the floor of the magma chamber. Such a dense layer would not mix with the overlying magma and could provide a suitable environment for the crystallization of large amounts of magnetite. However, this model requires fractionation of a large volume of magma, with formation of a considerably larger quantity of anorthosite than that observed in the Panzhihua intrusion. Faulting may have removed significant amounts of evolved rock at Panzhihua, which would influence the mass balance calculations. If the system was closed (see above), this negates the possibility that the oxides accumulated in a dynamic magma conduit such as that proposed for many magmatic sulfide deposits (e.g. Naldrett & Lightfoot, 1999; Lesher & Keays, 2002).

The massive ore bodies in the Panzhihua intrusion show clear intrusive boundaries with the silicate rocks in the Lower and Middle zones. The abundant Fe–Ti–V oxides (both magnetite and ilmenite) form intergranular to poikilitic masses enclosing or partly enclosing plagioclase and pyroxene, similar to that described for oxide ores in ODP Hole 735B (Robinson *et al.*, 2000; Hertogen *et al.*, 2002). In both occurrences, where they are in contact with oxides, the silicate minerals are rimmed with brown hornblende (Fig. 4). These textural relationships strongly support crystallization of the ilmenite and magnetite from an oxide melt that invaded a silicate crystal mush.

The Panzhihua ores occur as stratiform layers (Fig. 2), typical of magmatic deposits. In addition, the magnetite ores are associated with magmatic silicates and brown hornblende (Fig. 4), leaving little doubt that they are magmatic in origin and crystallized from oxide ore melts. Such oxide ore melts would be much denser than the silicate magmas and are therefore unlikely to have migrated from elsewhere. However, in Chile, Mexico, and Sweden (see discussion of nelsonites below), large concentrations of volatiles have been interpreted as 'propellants' responsible for emplacement of the melts. The presence of such volatiles has been recognized by

abundant apatite and fluid inclusions in the ore minerals. However, the Panzhihua oxide ores contain only minor apatite and amphibole. The most reasonable conclusion is that the ore liquids were produced within the magma chamber that produced the Panzhihua intrusion.

The origin of the Fe–Ti–V-rich oxide melts is uncertain, but we suggest that these melts formed as immiscible melts within the magma chamber and then settled to the bottom of the chamber, where they accumulated. Nelsonites, which are composed of massive iron oxides and apatite, have been reported in Chile (Park, 1961; Philpotts, 1967; Kolker, 1982; Nystrom & Henriquez, 1994), Mexico (Lyons, 1988), and Sweden (Williams, 1969). It has been documented that they formed directly from immiscible Fe–Ti–P oxide melts (Philpotts, 1967; Kolker, 1982; Nystrom & Henriquez, 1994; Ripley *et al.*, 1998; Clark & Kontak, 2004). They are usually associated with anorthosites or other alkaline rocks and may not be directly comparable with the oxides in Panzhihua. Reynolds (1985*b*) explained the formation of magnetite layers in the Bushveld complex from immiscible oxide melts. Von Gruenwaldt (1994) proposed that an immiscible Fe–Ti–Ca–P liquid was periodically developed in the topmost 1000 m of the Upper zone in the Bushveld complex, and that the development of the mineralized zones at the base of distinct geochemical cycles suggests formation of the immiscible melts by magma mixing.

The formation of an immiscible oxide melt from the silicate magma may have resulted from mineral fractionation, magma mixing, an abrupt change in oxygen fugacity, and/or an introduction of fluids. The presence of minor disseminated sulfides and apatite suggests that S and P may have acted as fluxing agents that facilitated development of the immiscible liquids. The association of amphibole and magnetite suggests that water and other fluids also played a part in this process. Water and CO_2-rich fluids may have been introduced through magma–wall-rock interaction during or after the emplacement of the high-Fe gabbroic magmas. The abundance of hydrous minerals in the oxide gabbros in the Panzhihua intrusion suggests that fluids were introduced into the system during crystallization.

SUMMARY AND CONCLUSIONS

The Panzhihua gabbroic layered intrusion shows both small-scale rhythmic layering and overall fractionation with increasing stratigraphic height. Mafic minerals, such as olivine and clinopyroxene, dominate in the lower parts of each rhythmic unit, whereas felsic minerals, such as plagioclase, are abundant at the top. Likewise, melanogabbros are most abundant in the Lower and Middle zones, whereas leucogabbros and more evolved rocks dominate in the Upper zone. The major oxide ore bodies are hosted in the Lower and Middle zones. The overall enrichment of Fe, V, and Ti in the Panzhihua intrusion indicates that the parental magmas were Fe-rich and Si-poor. Similar Fe–Ti oxide gabbros have been reported from the ocean crust and other localities on land.

The textural relationships between the Fe–Ti-rich gabbros and oxide ores in the Panzhihua intrusion support crystallization of the ilmenite and magnetite from oxide ore melts. The exact mechanism by which the oxide liquids formed is uncertain, but presumably involved concentration of Fe and Ti by fractional crystallization of ferrobasaltic or ferropicritic magmas followed by separation into silicate magma and Fe-rich oxide ore melt (Fig. 14). The abundance of hydrous minerals in these rocks points to the introduction of fluids into the system, which may have triggered immiscibility in melts already enriched in Fe and Ti.

The Panzhihua gabbros preserve rare, natural examples of late-stage liquids associated with the fractionation of tholeiitic or picritic magmas in a plutonic setting. Further study of these rocks should shed additional light on the processes of magmatic evolution and the formation of massive Fe–Ti–V oxide deposits.

ACKNOWLEDGEMENTS

This study was substantially supported by grants from the Research Grant Council of Hong Kong, China (HKU7056/03P). Additional support was provided by an Outstanding Young Researcher Award from the Chinese NSF (project 40129001) and a matching fund from The University of Hong Kong to M.-F.Z. We thank Professor Yuxiao Ma for providing assistance during our field work over the past several years, Ms Xiao Fu and Mr Liang Qi for help with analyses, and Mr Kwan Nang Pang, Dr Xieyan Song, Ms Christina Y. Wang and Mr Junhong Zhao for help with the preparation of this manuscript. Dr Peter C. Lightfoot is thanked for reading an earlier draft of this paper. We are also grateful to an anonymous referee, Professor Tony Naldrett and Dr Janina Wiszniewska for their constructive reviews.

REFERENCES

Barnes, S. J., Naldrett, A. J. & Gorton, M. (1985). The origin of the fractionation of platinum-group elements in terrestrial magmas. *Chemical Geology* **53**, 303–323.

Brooks, C. K. & Nielsen, T. F. D. (1978). Early stages in differentiation of Skaergaard magma as revealed by a closely related suite of dike rocks. *Lithos* **11**, 1–14.

Brooks, C. K., Larsen, I. M. & Nielsen, T. F. D. (1991). Importance of iron-rich tholeiitic magmas at divergent plate margins—a reappraisal. *Geology* **19**, 269–272.

Burchfiel, B. C., Chen, Z., Liu, Y. & Royden, L. H. (1995). Tectonics of the Longmenshan and adjacent regions, central China. *International Geology Review* **37**, 661–736.

Cabri, L. J. (ed.) (2002). *The Geology, Geochemistry, Mineralogy, Mineral Beneficiation of the Platinum-Group Elements. Canadian Institute of Mining, Metallurgy and Petroleum, Special Volume* **54**, 852 pp.

Campbell, I. H. (1977). Study of macro-rhythmic layering and cumulate processes in Jimberlana intrusion, Western Australia. 1. Upper layered series. *Journal of Petrology* **18**, 183–215.

Cawthorn, R. G. (ed.) (1996). *Layered Intrusions. Developments in Petrology* **15**, 531 pp.

Cawthorn, R. G. & Spies, L. (2003). Plagioclase content of cyclic units in the Bushveld Complex, South Africa. *Contributions to Mineralogy and Petrology* **145**, 47–60.

Chung, S. L. & Jahn, B. M. (1995). Plume–lithosphere interaction in generation of the Emeishan flood basalts at the Permian–Triassic boundary. *Geology* **23**, 889–892.

Clark, A. H. & Kontak, D. J. (2004). Fe–Ti–P oxide melts generated through magma mixing in the Antauta Subvolcanic Center, Peru: implications for the origin of nelsonite and iron oxide-dominated hydrothermal deposits. *Economic Geology* **99**, 377–395.

Compston, W., Williams, I. S. & Meyer, C. (1984). U–Pb geochronology of zircons from Lunar Breccia 73217 using a sensitive high mass-resolution ion microprobe. *Journal of Geophysical Research* **89**, 525–534.

Eales, H. V. & Cawthorn, R. G. (1996). The Bushveld complex. In: Cawthorn, R. G. (ed.) *Layered Intrusions*. Amsterdam: Elsevier, pp. 181–232.

Fornari, D. J., Perfit, M. R., Malahoff, A. & Embley, R. (1983). Geochemical studies of abyssal lavas recovered by DSRV ALVIN from Eastern Galapagos rift, INCA transform and Ecuador rift. 1. Major element variations in natural glasses and spatial distribution of lavas. *Journal of Geophysical Research* **88**, 519–529.

Hanski, E. J. (1992). Petrology of the Pechenga ferropicrites and cogenetic, Ni-bearing gabbro–wehrlite intrusions, Kola Peninsula, Russia. *Geological Survey of Finland Bulletin* **367**, 192 pp.

Hertogen, J., Emmermann, R., Robinson, P. T. & Erzinger, J. (2002). Lithology, mineralogy, and geochemistry of the lower ocean crust, ODP Hole 735B, Southwest Indian Ridge. In: *Proceedings of the Ocean Drilling Program, Scientific Results, 176 (CD-ROM)*. College Station, TX: Ocean Drilling Program.

Hunter, R. H. & Sparks, R. S. J. (1987). The differentiation of the Skaergaard intrusion. *Contributions to Mineralogy and Petrology* **95**, 451–461.

Irvine, T. N. (1975). Crystallization sequences in Muskox intrusion and other layered intrusions. 2. Origin of chromitite layers and similar deposits of other magmatic ores. *Geochimica et Cosmochimica Acta* **39**, 991–1020.

Irvine, T. N. (1977). Origin of chromitite layers in Muskox intrusion and other stratiform intrusions—new interpretation. *Geology* **5**, 273–277.

Irvine, T. N. (1988). Muskox intrusion, Northwest Territories. In: Hulbert, L. J., Duke, J. M., Eckstrant, O. R., Lydon, J. W., Scoates, R. F. J. & Cabri, L. J. (eds) *Geological Environments of the Platinum-Group Elements. Geological Survey of Canada Open File* **1440**, 25–39.

Irvine, T. N., Keith, D. W. & Todd, S. G. (1983). The J-M platinum–palladium reef of the Stillwater complex, Montana 2. Origin by double-diffusive convective magma mixing and implications for the Bushveld complex. *Economic Geology* **78**, 1287–1334.

Keays, R. R., Lesher, C. M., Lightfoot, P. C. & Farrow, C. E. G. (eds) (1999). *Dynamic Processes in Magmatic Ore Deposits and their Application in Mineral Exploration. Geological Association of Canada, Short Course Volume* **13**, 477 pp.

Kinnaird, J. A., Kruger, F. J., Nex, P. A. M. & Cawthorn, R. G. (2002). Chromitite formation—a key to understanding processes of platinum enrichment. *Transactions of the Institution of Mining and Metallurgy* **111**, 23–35.

Kolker, A. (1982). Mineralogy and geochemistry of Fe–Ti oxide and apatite (nelsonite) deposits and evaluation of the liquid immiscibilty hypothesis. *Economic Geology* **77**, 1146–1158.

Larsen, L. M., Watt, W. S. & Watt, M. (1989). *Geology and Petrology of the Lower Tertiary Plateau Basalts of the Scoresby Sund Region, East Greenland. Grønlands Geologiske Undersøgelse Bulletin* **157**, 164 pp.

Lee, C. A. (1996). A review of mineralization in the Bushveld complex and some other layered mafic intrusions. In: Cawthorn, R. G. (ed.) *Layered Intrusions*. Amsterdam: Elsevier, pp. 103–146.

Lesher, C. M. & Keays, R. R. (2002). Komatiite-associated Ni–Cu–(PGE) deposits. In: Cabri, L. J. (ed.) *The Geology, Geochemistry, Mineralogy, Mineral Beneficiation of the Platinum-Group Elements. Canadian Institute of Mining, Metallurgy and Petroleum, Special Volume* **54**, 579–618.

Lesher, C. M. & Stone, W. E. (1996). Exploration geochemistry of komatiites. In: Wyman, D. A. (ed.) *Igneous Trace Element Geochemical Applications for Massive Sulphide Exploration. Geological Association of Canada, Short Course Notes* **12**, 153–204.

Ludden, J. N., Thompson, G., Bryan, W. B. & Frey, F. A. (1980). The origin of lavas from the Ninety-East Ridge, eastern Indian Ocean—an evaluation of fractional crystallization models. *Journal of Geophysical Research* **85**(NB8), 4405–4420.

Lyons, J. I. (1988). Volcanogenetic iron oxide deposits, Cerro de Mercado and vicinity, Durango, Mexico. *Economic Geology* **83**, 1886–1906.

Ma, Y. X., Ji, X. T., Li, J. C., Huang, M. & Min, Z. Z. (2003). Mineral resources of Panzhihua, Sichuan Province, SW China. Chengdu: Chengdu University of Technology, 275 pp.

McBirney, A. R. (1996). The Skaergaard intrusion. In: Cawthorn, R. G. (ed.) *Layered Intrusions*. Amsterdam: Elsevier, pp. 147–180.

Melson, W. G. & O'Hearn, T. (1986). 'Zero-age' variations in the composition of abyssal volcanic rocks along the axial zone of the Mid-Atlantic Ridge. In: Vogt, P. R. & Tucholke, B. E. (eds) *The Geology of North America, Vol. M. The Western North Atlantic Region*. Boulder, CO: Geological Society of America, pp. 117–136.

Morse, S. A. (1980). Kiglapait geochemistry. IV. The major elements. *Geochimica et Cosmochimica Acta* **45**, 461–479.

Naldrett, A. J. & Lightfoot, P. C. (1999). Ni–Cu–PGE deposits of the Noril'sk region, Siberia; their formation in conduits for flood basalt volcanism. In: Keays, R. R., Lesher, C. M., Lightfoot, P. C. & Farrow, C. E. G. (eds) *Dynamic Processes in Magmatic Ore Deposits and their Application in Mineral Exploration. Geological Association of Canada, Short Course Volume* **13**, 195–249.

Nystrom, J. O. & Henriquez, F. (1994). Magmatic features of iron ores of the Kiruna type in Chile and Sweden: ore textures and magnetite geochemistry. *Economic Geology* **89**, 820–839.

Park, C. F. (1961). A magnetite lava 'flow' in Northern Chile. *Economic Geology* **56**, 431–441.

Parks, J. & Hill, R. E. T. (1986). Phase compositions and cryptic variation in a 2·2 km section of the Windimurra layered gabbroic intrusion, Yilgarn block, Western Australia—a comparison with the Stillwater complex. *Economic Geology* **81**, 1196–1202.

Parsons, I. (ed.) (1987) *Origins of Igneous Layering. NATO ASI Series, C 196*. Dordrecht: D. Reidel, 666 pp.

Pearce, J. A. & Norry, M. J. (1979). Petrogenetic implications of Ti, Zr, Y, and Nb variations in volcanic rock. *Contributions to Mineralogy and Petrology* **69**, 33–47.

Philpotts, A. R. (1967). Origin of certain iron–titanium oxide and apatite rocks. *Economic Geology* **62**, 303–315.

Reynolds, I. M. (1978). Mineralogical studies of South African titaniferous iron ores: their applications to extractive metallurgy. *Transactions of the Geological Society of Africa* **81**, 233–240.

Reynolds, I. M. (1985*a*). The nature and origin of titaniferous magnetite-rich layers in the upper zone of the Bushveld complex: a review and synthesis. *Economic Geology* **80**, 1089–1108.

Reynolds, I. M. (1985*b*). Contrasting mineralogy and textural relationships in the uppermost titaniferous magnetite layers of the Bushveld complex in the Bierkraal area north of Rusternburg. *Economic Geology* **80**, 1027–1048.

Ripley, E. M., Severson, M. J. & Hauck, S. A. (1998). Evidence for sulfide and Fe–Ti–P-rich liquid immiscibility in the Duluth Complex, Minnesota. *Economic Geology* **93**, 1052–1062.

Robinson, P. T., Dick, H. J. B., Natland, J. H. & ODP Leg 176 Shipboard Party (2000). Lower oceanic crust formed at an ultra-slow-spreading ridge: Ocean Drilling Program Hole 735B, Southwest Indian Ridge. In: Dilek, Y., Moores, E. M., Elthon, D. & Nicolas, A. (eds) *Ophiolites and Ocean Crust: New Insights from Field Studies and the Ocean Drilling Program*. *Geological Society of America, Special Papers* **349**, 75–86.

Rollison, H. R. (1993). *Using Geochemical Data: Evaluation, Presentation, Interpretation*. Singapore: Longman, 352 pp.

SBGMR (Sichuan Bureau of Geology and Mineral Resources) (1991). *Regional Geology of Sichuan Province*. Beijing: Geological Publishing House, 680 pp. (in Chinese).

Scoon, R. N. & Mitchell, A. A. (1994). Discordant iron-rich ultramafic pegmatites in the Bushveld complex and their relationship to iron-rich intercumulus and residual liquids. *Journal of Petrology* **35**, 881–917.

Song, X. Y., Zhou, M.-F., Hou, Z. Q., Cao, Z., Wang, Y. & Li, Y. (2001). Geochemical constraints on the mantle source of the Upper Permian Emeishan continental flood basalts, southwestern China. *International Geology Review* **43**, 213–225.

Song, X. Y., Zhou, M.-F., Cao, Z., Sun, M. & Wang, Y. (2003). Ni–Cu–(PGE) magmatic sulfide deposits in the Yangliuping area, Permian Emeishan Large Igneous Province, SW China. *Mineralium Deposita* **38**, 831–843.

Sun, S. S. & McDonough, W. F. (1989). Chemical and isotopic systematics of oceanic basalts: implications for mantle composition and processes. In: Saunders, A. D. & Norry, M. J. (eds) *Magmatism in the Ocean Basins*. *Geological Society, London, Special Publications* **42**, 313–345.

Tang, H. S. (1984). The Panzhihua V–Ti–magnetite deposits. In: Panxi Geological Team of Sichuan Geological Survey (eds) *Research Report of Metallogeny and its Prediction* (unpublished) (in Chinese).

Taylor, S. R. & McLennan, S. M. (1985). *The Continental Crust: its Composition and Evolution*. Oxford: Blackwell, 312 pp.

Von Gruenwaldt, G. (1994). Ilmenite–apatite enrichment in the upper zone of the Bushveld complex: a major titanium–rock phosphate resource. *International Geology Review* **35**, 987–1000.

Wager, L. R. & Brown, G. M. (1968). *Layered Igneous Rock*. Edinburgh: Oliver & Boyd, 588 pp.

Weaver, B. L. (1990). Geochemistry of highly-undersaturated ocean island basalt suites from the South Atlantic Ocean: Fernando de Noronha and Trinidade islands. *Contributions to Mineralogy and Petrology* **105**, 502–515.

Wiebe, R. A. (1979). Fractionation and liquid immiscibility in an anorthositic pluton of the Nain complex, Labrador. *Journal of Petrology* **20**, 239–269.

Wiebe, R. A. (1997). Fe-rich tholeiitic liquids and their cumulate products in the Pleasant Bay layered intrusion, Coastal Maine. *Contributions to Mineralogy and Petrology* **129**, 255–267.

Williams, D. (1969). Ore deposits of volcanic affilation. In: James, C. H. (ed.) *Sedimentary Ores Ancient and Modern (Revised)*. *Geological Department, Leicester, Special Publication* **1**, 197–206.

Wilson, M. (1989). *Igneous Petrogenesis*. London: Unwin Hyman, 494 pp.

Winter, P. E. (1965). *The Ushushwana Igneous Complex*. *Swaziland Geological Survey Bulletin* **5**, 29 pp.

Xu, Y. G., Chung, S. L., Jahn, B. M. & Wu, G. Y. (2001). Petrologic and geochemical constraints on the petrogenesis of Permian–Triassic Emeishan flood basalts in southwestern China. *Lithos* **58**, 145–168.

Yan, D. P., Zhou, M. F., Song, F. & Fu, Z. (2003). Structural style and tectonic significance of the Jianglang metamorphic core complex in the eastern margin of the Tibetan Plateau, China. *Journal of Structural Geology* **25**, 239–254.

Zhang, Y. X., Lou, Y. & Yang, X. (1988). *The Panxi Rift*. Geological Press, Beijing, 422 pp. (in Chinese).

Zhong, H., Zhou, X. H., Zhou, M.-F., Sun, M. & Liu, B. G. (2002). Platinum-group element geochemistry of the Hongge layered intrusion in the Pan-Xi area, southwestern China. *Mineralium Deposita* **37**, 226–239.

Zhong, H., Yao, Y., Hu, S. F., Zhou, X. H., Liu, B. G., Sun, M., Zhou, M.-F. & Viljoen, M. J. (2003). Trace-element and Sr–Nd isotopic geochemistry of the PGE-bearing Hongge layered intrusion, southwestern China. *International Geology Review* **45**, 371–382.

Zhou, M.-F., Yang, Z. X., Song, X. Y., Keays, R. R. & Lesher, C. M. (2002*a*). Magmatic Ni–Cu–(PGE) sulfide deposits in China. In: Cabri, L. J. (ed.) *The Geology, Geochemistry, Mineralogy, Mineral Beneficiation of the Platinum-Group Elements*. *Canadian Institute of Mining, Metallurgy and Petroleum, Special Volume* **54**, 619–636.

Zhou, M.-F., Yan, D. P., Kennedy, A. K., Li, Y. Q. & Ding, J. (2002*b*). SHRIMP zircon geochronological and geochemical evidence for Neoproterozoic arc-related magmatism along the western margin of the Yangtze Block, South China. *Earth and Planetary Science Letters* **196**, 51–67.

Zhou, M.-F., Malpas, J., Song, X., Kennedy, A. K., Robinson, P. T., Sun, M., Lesher, C. M. & Keays, R. R. (2002*c*). A temporal link between the Emeishan large igneous province (SW China) and the end-Guadalupian mass extinction. *Earth and Planetary Science Letters* **196**, 113–122.